

# Effect of mechanical heterogeneity in arc crust on volcano deformation with application to Soufrière Hills Volcano, Montserrat, West Indies

Stefanie Hautmann,<sup>1</sup> Joachim Gottsmann,<sup>1</sup> R. Stephen J. Sparks,<sup>1</sup> Glen S. Mattioli,<sup>2</sup> I. Selwyn Sacks,<sup>3</sup> and Michael H. Strutt<sup>4</sup>

Received 26 August 2009; revised 7 March 2010; accepted 31 March 2010; published 9 September 2010.

[1] Analyses of volcano surface deformation are commonly based on models that assume mechanical homogeneity of rocks surrounding the causative pressure source. Here we present a detailed study that shows the differences in deduced surface deformation caused by source pressurization accounting for either mechanical homogeneity or mechanical heterogeneity of encasing rocks in a volcanic arc setting using finite element models. Accounting for crustal heterogeneity from seismic data, we test for a range of source geometries and intermediate crustal depths and explore the misfits of deduced source parameters from the two families of models. In the second part of this study, we test the results from the generic study against cGPS data from two deformation periods (the 2003–2005 ground inflation and the 2005–2007 ground deflation) at Soufrière Hills Volcano, Montserrat, West Indies, to inform on source parameters. Accounting for a variable crustal rigidity with depth as deduced by seismic analysis beneath Montserrat, we find the data to be best explained by pressurization and depressurization of a slightly prolate midcrustal magma chamber that is centered between 11.5 and 13 km below sea level, about 640 m NE of the active vent. Considering source dimension and source pressure changes, we demonstrate that magma compressibility and viscoelasticity of host rocks considerably affect dynamics in the midcrustal magmatic system of Soufrière Hills Volcano and need to be accounted for as first-order effects in geodetic data analyses and modeling.

**Citation:** Hautmann, S., J. Gottsmann, R. S. J. Sparks, G. S. Mattioli, I. S. Sacks, and M. H. Strutt (2010), Effect of mechanical heterogeneity in arc crust on volcano deformation with application to Soufrière Hills Volcano, Montserrat, West Indies, *J. Geophys. Res.*, 115, B09203, doi:10.1029/2009JB006909.

## 1. Introduction

[2] Geodetic studies of ground deformation in volcanic areas include the construction of models to help constrain parameters such as location, geometry and pressure change of causative sources. Deformation modeling has advanced from the pioneering approaches of Anderson [1936] and Mogi [1958] to models accounting for complex source geometries [e.g., Dieterich and Decker, 1975; Okada, 1985; Yang et al., 1988; Fialko et al., 2001], elastic heterogeneity [Rundle, 1980; Bianchi et al., 1984, 1987; Fernández and Rundle, 1994], structural discontinuities [De Natale and Pingue, 1993; Folch and Gottsmann, 2006], rheological differences [Bonafede et al., 1986; Fernández et al., 2001] and topography [Cayol and Cornet, 1998; Williams and

Wadge, 1998]. The interested reader is referred to the recent review by Poland et al. [2006] for a more detailed account of these models.

[3] Only few studies, however, investigate the combined influence of two or more of these factors on ground deformation [e.g., De Natale and Pingue, 1993; Folch et al., 2000]. For the specific case of elastic heterogeneity, Fernández and Rundle [1994] and Trasatti et al. [2003] studied the generic effect of varying the depth of a spherical pressure source in a multilayered elastic medium. Manconi et al. [2007] and Geyer and Gottsmann [2010] theoretically investigated the effect of layering of mechanically stiff and soft layers on surface deformation triggered from sources at shallow depths (up to 5 km). While Manconi et al. [2007] only accounted for a single spherical source, Geyer and Gottsmann [2010] also considered source multiplicity. Other works focus on effects of crustal heterogeneity on ground deformation at specific volcanoes such as Campi Flegrei, Mount Etna, and Okmok Volcano [Bonaccorso et al., 2005; Trasatti et al., 2005, 2008; Masterlark, 2007]. A key finding of studies comparing displacements in mechanical homogeneous versus heterogeneous crust is that source depths deduced by accounting for crustal heterogeneity differ from those assuming elastic

<sup>1</sup>Department of Earth Sciences, University of Bristol, Bristol, UK.

<sup>2</sup>Department of Geosciences, University of Arkansas, Fayetteville, Arkansas, USA.

<sup>3</sup>Department of Terrestrial Magnetism, Carnegie Institution of Washington, Washington, D. C., USA.

<sup>4</sup>British Geological Survey, Kingsley Dunham Centre, Keyworth, UK.

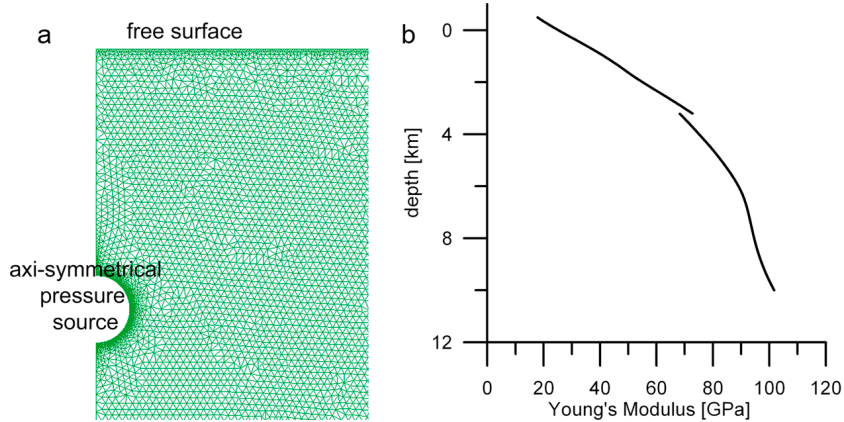


**Figure 1.** (a) Axially symmetric finite element model (only  $13 \times 10$  km is shown; the entire domain is  $100 \times 100$  km). The surface is assumed to be flat, while source depth, volume and geometries are varied (see text for details). The source is uniformly pressurized. (b) Young's modulus values for the upper crust as obtained from a  $P$  wave velocity model from Montserrat. Elastic heterogeneities are parameterized to increase gradually with depth.

mechanical homogeneity of country rock. Most studies, however, compare only results from models invoking a spherical pressure source. Though, there are few studies that compare (1) the influence of changing source geometries and (2) the effect of mechanical homogeneity versus heterogeneity [Battaglia and Segall, 2004; Pritchard and Simons, 2004], these factors are not combined in the modeling, but only analyzed separately. Hence, a full parameterization of differences in inferred source characteristics, including source depths, volumes and in particular shapes, when investigating ground deformation in a mechanically heterogeneous versus homogeneous medium, is lacking. As a result our knowledge on the combined influence of both parameters on surface deformation is incomplete. This paper serves as a first order parameterization of the combined effect of source geometry and mechanical heterogeneity on surface deformation by simulating pressurization of a midcrustal magma chamber.

[4] We first present a set of generic ground deformation models based on isotropic homogeneous elastic half-space (HOHS) and heterogeneous elastic half-space (HEHS) approaches, and show resulting differences in surface deformation when (1) accounting for elastic heterogeneities of host rocks in an island arc setting and (2) using simple assumptions for crustal mechanical properties. This study investigates differences on the horizontal and vertical component of the deformation field and accounts for the first time for a variety of source geometries and source depths in a heterogeneous medium. Second, we analyze continuous Global Positioning System (cGPS) data recorded during two eruption periods (2003–2005 during ground inflation, 2005–2007 during ground deflation) at Soufrière Hills Volcano (SHV), Montserrat, West Indies. We compare the observed displacements with results from our generic models to assess the role of a midcrustal magma reservoir during ground deformation and then fit the observables via a set of forward models to inform on its source characteristics.

[5] We provide a detailed study of surface deformation caused by the deep magma system beneath SHV that accounts for both crustal heterogeneities and anisotropies as

well as a finite magma body geometry. We thus build on the understanding of the structure of the SHV magmatic system inferred previously from ground deformation data [e.g., Mattioli et al., 1998; Voight et al., 2006; Wadge et al., 2006; Elsworth et al., 2008; Hautmann et al., 2009].

## 2. Theory

### 2.1. Method, Model Setup, and Calibration

[6] We use a finite element method to construct a set of generic models to simulate ground deformation induced by an axially symmetric, uniformly pressurized source in the mid crust (see Figure 1). We first investigate sources centered at a depth  $z = 11$  km (assuming  $z$  positive downward and  $z = 0$  at sea level) with spherical, oblate ( $c/a = 0.6$ , with axis  $a = b > c$ ) and prolate ( $a/c = 0.6$  with axis  $a = b < c$ ) geometries, respectively, and a volume of  $V = 14$  km $^3$  (corresponding to a radius  $r = 1.5$  km in a spherical source). We then vary individual source parameters, including the source volume ( $V = 9$  km $^3$  [ $r = 1.3$  km] and  $V = 21$  km $^3$  [ $r = 1.7$  km]), depth ( $z = 8$  km and  $z = 14$  km), and the eccentricity of the spheroidal sources ( $c/a = 0.8, 0.4, 0.2$  for oblate geometry,  $a/c = 0.8, 0.4, 0.2$  for prolate geometry). Furthermore, we simulate pressurization in a sill and a dike, respectively, centered at 11 km depth with a half-width of 100 m and a half-length of 3 km. The model parameters to illustrate generic surface deformation triggered by midcrustal magma chambers have been chosen based on source characteristics typically found in island arc volcano settings (e.g., source depths between 9 and 13 km at Miyakejima [Saito et al., 2005], Augustine Volcano [Cervelli and Coombs, 2006], Soufrière Hills Volcano [Mattioli and Herd, 2003]).

[7] In all our models, the free surface is assumed to be flat at  $z = -500$ . While this value is chosen somewhat arbitrarily, it nonetheless provides a reasonable approach for fitting measured GPS data with respect to the average elevation of a network in an island arc setting. The idealization of a flat surface is warranted, as the effect of topography on the deformation pattern decreases with increasing depth of the pressure source [Cayol and Cornet, 1998]. The axes of

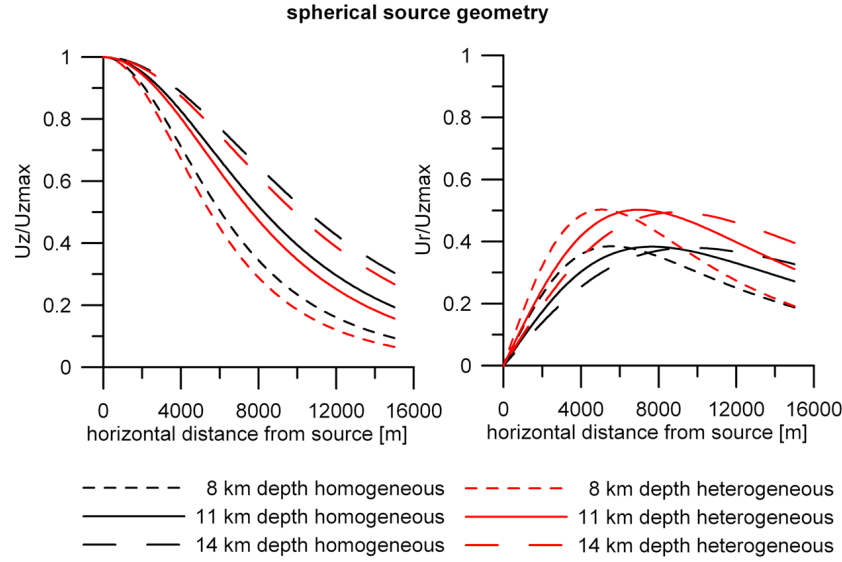


**Figure 2.** Normalized results of surface deformation due to overpressure in a spherical source at different depths. Results are shown for (left) vertical and (right) horizontal displacements in a homogeneous (black) and heterogeneous (red) medium. The predicted relative horizontal displacements are amplified in the heterogeneous model. At the same time, the source depth, inferred from the relative vertical deformation, is underestimated by 1.1 km, when erroneously assuming mechanical homogeneity.

the spheroidal sources are normal and parallel to the surface, respectively. The effective computational size of the generated models is large enough ( $100 \times 100$  km) to avoid boundary effects in the zone of interest.

[8] Solutions for the HOHS models are obtained for Young's Modulus ( $E$ ) and Poisson's ratio ( $\nu$ ) set constant at  $E = 75$  GPa and  $\nu = 0.25$ . Mechanical properties for the HEHS approach are inferred from data of seismic velocity profiles in the upper crust of island arc volcanoes. We have chosen a vertical 2-D  $P$ -wave velocity profile from the upper crust beneath the island of Montserrat [Paulatto et al., 2010], but note that this profile is very similar to those observed in other arc volcanoes (e.g., Popocatepetl [De Barros et al., 2008], Aso Volcano [Sudo and Kong, 2001]). In fact, we found that differences in between velocity models from Montserrat, Popocatepetl, and Aso Volcano, hence, differences in the inferred mechanical properties of the crust have only very minor effects on surface deformation. Thus, the results presented here are not site-specific to Montserrat, but broadly applicable. We assumed a Poisson's ratio  $\nu = 0.25$ , which yields values of Young's Modulus of 17 GPa  $\leq E \leq 102$  GPa for  $-0.5 \text{ km} \leq z \leq 10 \text{ km}$  (Figure 1). The sensitivity of the Young's Modulus on the value of the Poisson's ratio is low, for example, if one assumed  $\nu = 0.3$ , the resulting values for  $E$  would be increased by approximately 3%. Mechanical heterogeneity is not generated by superimposing mechanically different homogeneous layers onto each other to construct the model, but rather by assigning property values that gradually change with depth to each node of the finite element mesh. We here use the relation

$$\begin{aligned} E(z) = & 2.87 \times 10^{-19} z^5 + 1.55 \times 10^{-14} z^4 + 1.89 \times 10^{-10} z^3 \\ & - 2.33 \times 10^{-7} z^2 - 0.02z + 14 \end{aligned} \quad (1)$$

in order to describe  $E$  as a function of depth. As deduced from the Montserrat velocity profile, elastic properties tend to change only slightly at greater depths (see also Figure 1). Since our investigated source depths are not deeper than 14 km, we set  $E = 105$  GPa for  $z > 10$  km. Equations of linear elasticity have been solved numerically via a finite element (FE) method [Codina and Folch, 2004].

[9] We calibrated our FE approximation to analytical solutions of the Mogi model [Mogi, 1958]. While the FE method is based on the modeling of a finite source, the Mogi model assumes a point-source. However, Mogi [1958] demonstrated that a spherical body, which radius is far smaller than its depth may be represented by the mathematical concept of a point source. Expressions for a finite spherical source are given by McTigue [1987]. We tested both model approximations against each other for the example of a spherical source located at 11 km depth with a radius of 1 km and a uniform pressurization of 15 MPa. Elastic properties of the medium are set as  $E = 75$  GPa and  $\nu = 0.25$ . The FE method solution underestimates the Mogi solution for vertical and horizontal displacements by 0.3% only, which is an acceptable misfit.

## 2.2. Results

[10] We normalize results for vertical and horizontal displacements relative to the maximum vertical deformation  $U_{z\max}$ . Thus, the results are independent of source overpressure and differences between the HOHS and HEHS models. The presented plots can thus be applied to analyze deformation data from other volcanoes in similar settings in a straight-forward manner.

### 2.2.1. Spherical Sources

[11] Results from the HOHS approach using a spherical pressure source can be regarded as "Mogi-type" solutions. Figure 2 compares the differences to the HEHS models and

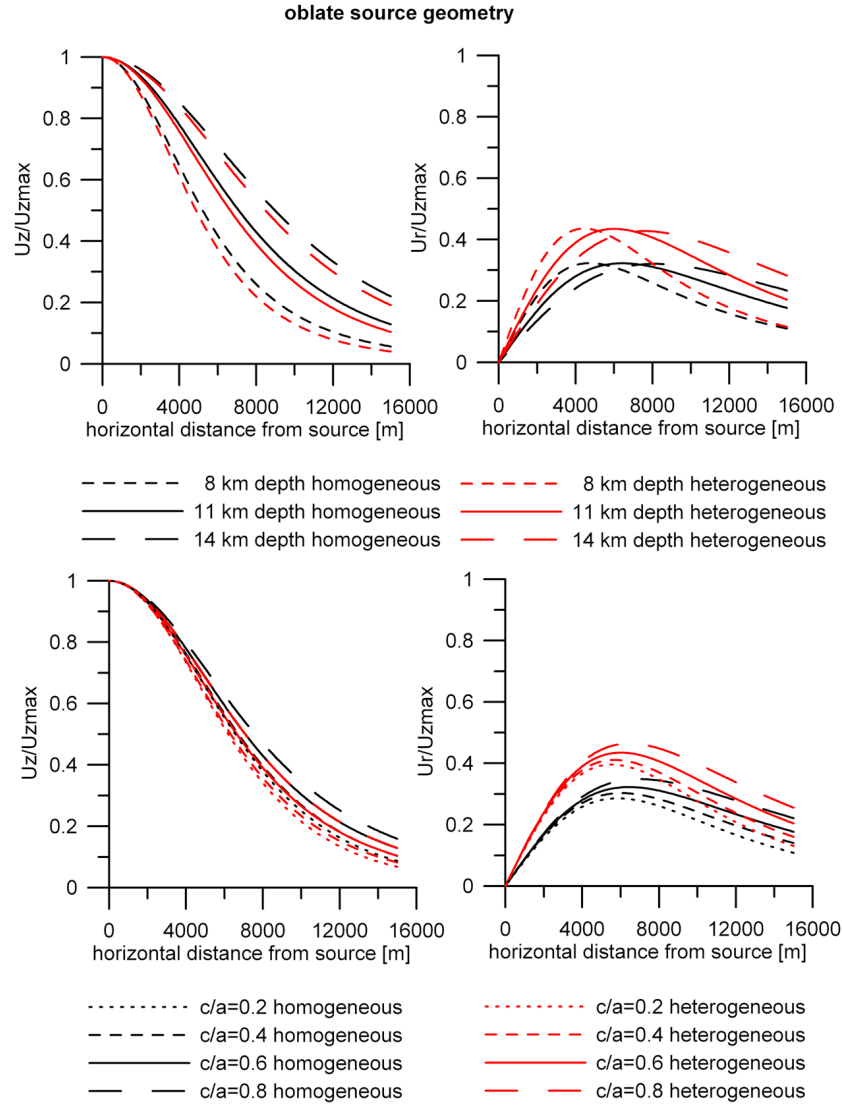


**Figure 3.** Normalized results of surface deformation induced by a pressurized oblate source. Results are shown for (left) vertical and (right) horizontal displacements in a homogeneous (black) and heterogeneous (red) medium. (top) Source geometry is assumed to be constant ( $c/a = 0.6$ ), while source depth is varied ( $z = 8 \text{ km}, 11 \text{ km}, \text{ and } 14 \text{ km}$ ). (bottom) Source depth is set at  $z = 11 \text{ km}$ , while different eccentricities ( $c/a = 0.2, 0.4, 0.6, \text{ and } 0.8$ ) of the oblate source are tested. Smaller values of  $c/a$  correlate with higher source eccentricity and vice versa,  $c/a = 1$  corresponds to a source of spherical shape.

represents the misfit in the classic Mogi model when applied to comparable geologic settings. The results reveal two significant differences between the two models. First, the predicted normalized maximum horizontal surface deformation  $U_{rmax}$  is amplified by 31% when accounting for heterogeneity. This leads to an increase in  $U_{rmax}/U_{zmax}$  of 0.12. Varying the values for source depth and volume gives only a small difference of  $\pm 0.003$  in  $U_{rmax}/U_{zmax}$ . The amplification of horizontal surface deformation becomes less significant at larger distances from the source, due to a stronger signal decay in a heterogeneous medium. Second, the predicted wavelength, i.e., the footprint of vertical surface deformation decreases when employing a heterogeneous model. This is reflected (1) in a shortening of the radial distance to  $U_{rmax}$  by  $0.7 \text{ km} \pm 0.1 \text{ km}$  (with a larger distance for increasing  $z$ ) and (2) in a steeper decrease of  $U_z$

with distance from source. Note that we report distance here as the distance to the source center projected to the free surface. For the same pressure increment the reduction of the footprint would derive in a source depth reduced by about 1.1 km (for sources centered between 8 and 14 km depth) compared to the HOHS solutions.

## 2.2.2. Oblate Sources

[12] Our results show that in HEHS models an oblate source gives lower amplitude horizontal displacements compared to a spherical source (Figure 3). This finding is in agreement with previous results for HOHS models [Dieterich and Decker, 1975]. This effect, although significant when applying a HEHS model, is reduced, however, as the predicted relative maximum horizontal deformation is amplified by 35% (for  $c/a = 0.6$ ; while 36% for  $c/a = 0.2$ ). This corresponds to an increase of  $U_{rmax}/U_{zmax}$  by 0.11 (for

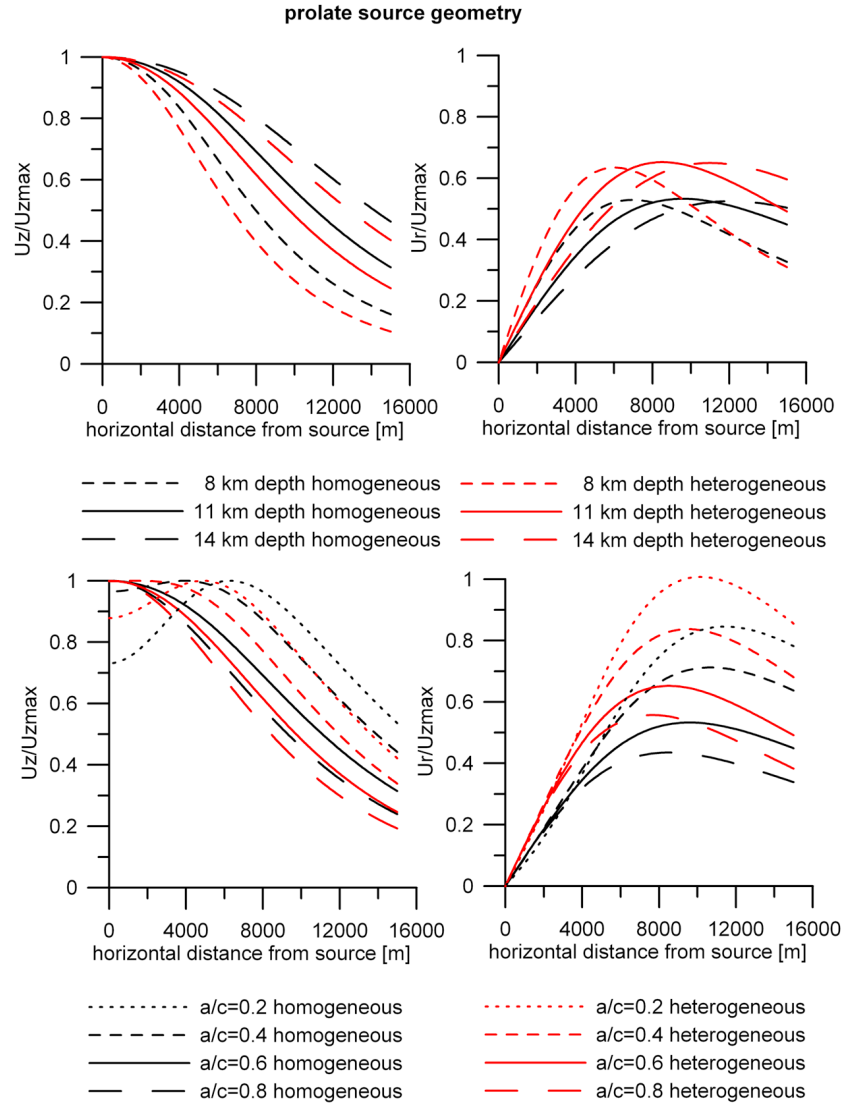


**Figure 4.** Normalized results of surface deformation induced by a pressurized prolate source. Results are shown for (left) vertical and (right) horizontal displacements in a homogeneous (black) and heterogeneous (red) medium. (top) Source geometry is assumed to be constant ( $a/c = 0.6$ ), while source depth is varied ( $z = 8$  km, 11 km, and 14 km). (bottom) Source depth is set at  $z = 11$  km, while different eccentricities ( $a/c = 0.2, 0.4, 0.6$ , and 0.8) of the prolate source are tested. Smaller values of  $a/c$  correlate with higher source eccentricity and vice versa,  $a/c = 1$  corresponds to a source of spherical shape.

$c/a = 0.6$ ; while 0.1 for  $c/a = 0.2$ ) in the heterogeneous model. The resulting horizontal distance  $U_{r\max}$  to source center decreases by 0.4–0.7 km in the heterogeneous model, with  $U_{r\max}$  closer to the source at higher eccentricity or greater depth of the source. The relative vertical deformation predicted by the heterogeneous model corresponds to the predicted relative vertical deformation from a source located 1.0 km shallower in a homogeneous model. Predicted deformation patterns for the sill geometry are equal to solutions for the oblate spheroidal source with  $c/a = 0.2$  and therefore are not shown separately.

### 2.2.3. Prolate Sources

[13] Surface displacements induced by a prolate source show that increasing eccentricity of the source causes more horizontal deformation and larger distances between source center and  $U_{r\max}$  (Figure 4). Applying the heterogeneous

model results in a relative maximum horizontal deformation increased of 25% (for  $a/c = 0.6$ ; 19% for  $a/c = 0.2$ ), which leads to a change in  $U_{r\max}/U_{z\max}$  of 1.2 (for  $a/c = 0.6$ ; 1.6 for  $a/c = 0.2$ ). The radial distance  $U_{r\max}$  to source center decreases by 0.7–1.3 km, with  $U_{r\max}$  closer to the source at a smaller eccentricity or greater source depth. The predicted vertical deformation pattern derived from the heterogeneous model corresponds to the solution obtained from the homogeneous model with a source located about 1.3 km shallower. A dike centered in the mid crust did not give any significant surface deformation (i.e., <1 mm) in our models.

### 2.2.4. Effect of Mechanical Heterogeneity on Absolute Displacements

[14] Generic relations between differences in the predicted magnitude of absolute vertical deformation when employing a heterogeneous versus homogeneous model cannot be

given, as the ratio  $U_{zmax}$  homogeneous medium/ $U_{zmax}$  heterogeneous medium depends solely on the elastic property values chosen for the homogeneous model. Comparison of the ratios  $U_{zmax}$  homogeneous medium/ $U_{zmax}$  heterogeneous medium for a range of different source shapes to examine any relative dependence with respect to changing source geometries did not reveal any correlation, and therefore the results are not shown.

### 2.3. Discussion

[15] In summary, we found three significant discrepancies between the predicted deformation pattern obtained from models using a purely homogeneous medium and a medium with rock properties that change systematically as function of depth.

[16] First, the predicted horizontal displacement from a pressurized source is markedly amplified by mechanical heterogeneity. To fit observables, one would therefore deduce more prolate source geometries in models accounting for mechanical homogeneity only. The effect is even more pronounced for prolate sources in a heterogeneous medium, but attenuates slightly for oblate sources.

[17] Second, the maximum horizontal deformation at the free surface occurs closer to the source in a heterogeneous medium. The more prolate the source and/or the deeper the source, the more significant the effect. The more oblate and/or the shallower the source the less significant the effect.

[18] Third, the wavelength (footprint) of vertical surface deformation is shorter in a heterogeneous medium. The shortening corresponds to an underestimation of source depth by 1.0–1.3 km, when accounting for mechanical homogeneity. The disparity increases for prolate source geometries compared to oblate ones.

[19] In summary, we conclude that misfits between solutions from homogeneous and heterogeneous models vary only slightly between oblate and spherical sources, while for prolate sources the misfits differ more strongly. The effect of varying source volumes over the range described above only result in very minor discrepancies between either solution and can hence be neglected. Note, however, that when applying velocity models from different tectonic settings, the qualitative observations described should be similar, although some minor quantitative variations might occur.

[20] We found that the difference between the heterogeneous and the homogeneous model solutions (shown in Figures 2–4) did not depend on the depth of the source for depths greater 11 km. There are very minor differences for shallower sources, but they are likely below the detection limit for most surveillance techniques. However, the effect of topographic relief increases for sources at shallower depths.

## 3. Model Application to Deformation at Soufrière Hills Volcano, Montserrat, West Indies

### 3.1. Background Information on the Volcano's Magmatic System

[21] Soufrière Hills Volcano (SHV; Montserrat, West Indies) is currently one of the most active dome-building andesitic volcanoes on Earth [e.g., Wadge *et al.*, 2006]. Since the beginning of its eruption in 1995, one scientific challenge has been to link explosive and effusive eruptive phenomena

with physico-chemical processes with its plumbing system at depth. Numerous studies have been conducted using geo-physical and petrological data, in addition to the development of theoretical models on fluid flow dynamics, in order to assess the structure and dynamics of the complex shallow and deep magmatic system of SHV.

[22] 1. *Mattioli et al.* [1998], *Costa et al.* [2007a, 2007b], *Hautmann et al.* [2009], and *Linde et al.* [2008] proposed the shallow feeding system at SHV to consist of a vertical dike-conduit system trending NW-SE to NNW-SSE. The presence of a shallow dike beneath SHV was first proposed by *Mattioli et al.* [1998], on grounds of inversion of recorded ground deformation data. Detailed studies of fluid flow dynamics (to constrain source geometry and over-pressure values [*Costa et al.*, 2007a, 2007b]) combined with 3-D models of surface deformation (accounting for topography, host rock heterogeneity and finite source geometry [*Hautmann et al.*, 2009]) and comparisons with tiltmeter records further constrained the dike to roughly 500 m in horizontal length with a thickness of ca. 2 m. At depths shallower than 1 km the dike is proposed to open into a cylindrical conduit with a radius of ca. 15 m at the surface [*Sparks et al.*, 2000]. Analysis of recent strainmeter data [*Linde et al.*, 2008] is also consistent with the dike model.

[23] 2. The shallow dike-conduit is assumed to couple to a magma reservoir which top is at about 5 km depth. Inversion of geodetic data for a pressurized spherical source embedded in a homogeneous elastic half-space [*Mogi*, 1958] that were recorded in the early stage of the eruption (1995–1997) indicated the magma chamber to be centered at about 6 km depth beneath the Soufrière Hills crater [*Mattioli et al.*, 1998]. Additional studies using data from borehole dilatometers [*Voight et al.*, 2006], petrological observations [*Murphy et al.*, 2000; *Devine et al.*, 2003], and experimental phase equilibria studies [*Barclay et al.*, 1998; *Couch et al.*, 2003; *Rutherford and Devine*, 2003] further supported the inferred location of the top of the shallow magma reservoir and constrained the chamber to be a slightly flattened spheroidal source with an estimated volume of 4 km<sup>3</sup>.

[24] 3. The evaluation of cGPS data from subsequent phases of the eruption (2003–2007) indicated that the observed surface deformation may be explained by pressure variations in a spherical source that is centered between 9 and 13 km depth with an estimated volume of 4 km<sup>3</sup> [*Mattioli and Herd*, 2003; *Mattioli*, 2005]. *Voight et al.* [2008] proposed a prolate spheroidal magma reservoir (a/c = 0.5) located at about 10 km depth. Petrological data (basalt inclusions in the erupted andesites) support the principle assumption of a deeper mafic reservoir that is connected via a conduit to the upper chamber [*Murphy et al.*, 2000; *Devine et al.*, 2003; *Annen et al.*, 2006].

[25] The emerging picture is that the current eruption of SHV is fed by multiple reservoirs, i.e., two stacked magma chambers, [e.g., *Elsworth et al.*, 2008]. Current results from the analysis using cGPS data should, however, be regarded as first order approximations, as computational simulations are built on simplistic assumptions as to the mechanical properties of the subsurface beneath Montserrat. To our knowledge, ground deformation models based on a more realistic account of rock mechanics to evaluate the possible role of a deeper reservoir for the recorded ground defor-

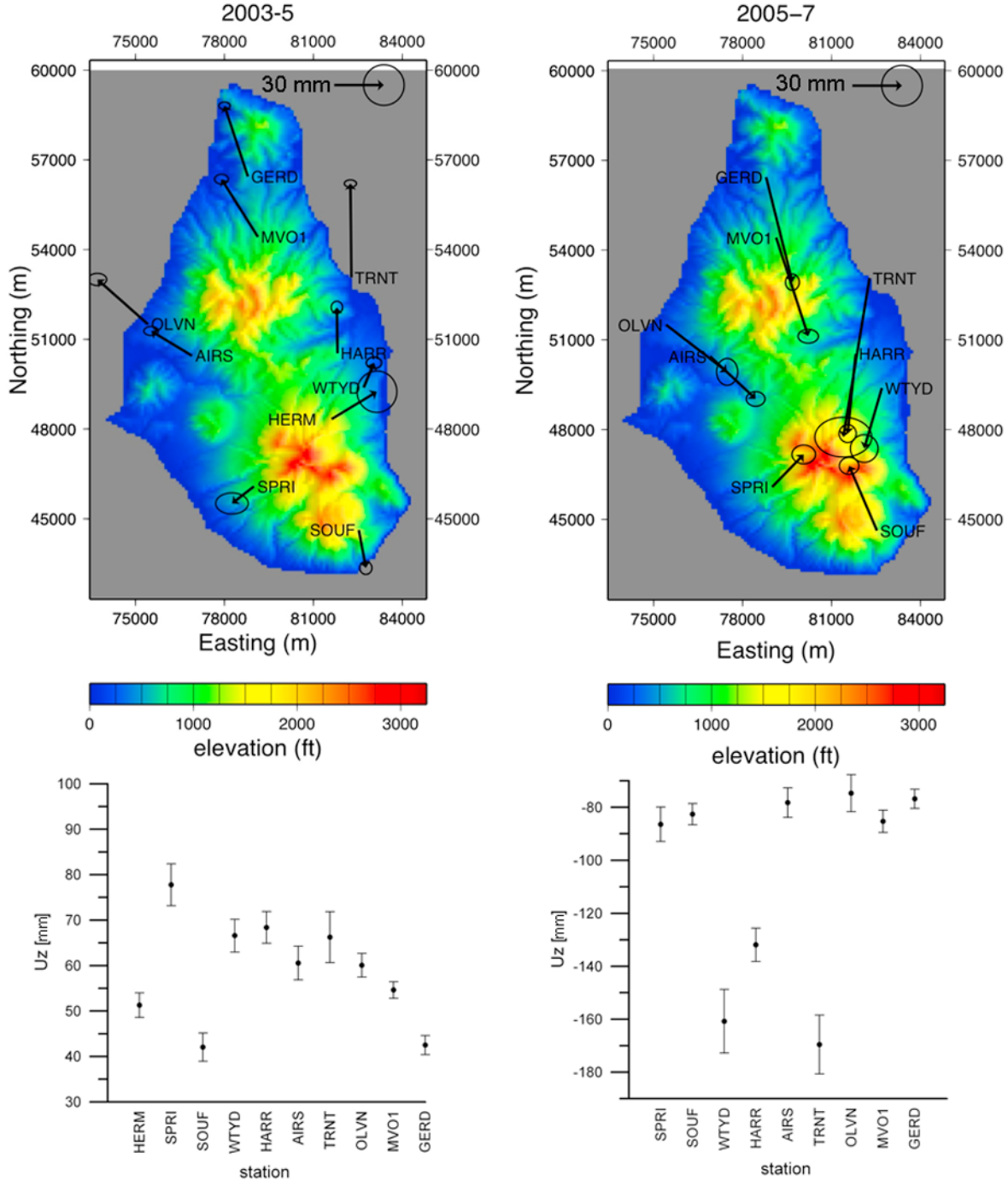


**Figure 5.** (top) Map of Montserrat, West Indies, showing the locations of the cGPS sites and recorded horizontal surface deformation including measure uncertainties. (left) Deformation data cover one entire period of ground inflation (July 2003 to November 2005), and (right) the subsequent episode of ground deflation (December 2005 to March 2007). (bottom) Corresponding vertical deformation as recorded at each station. Stations are listed in order of distance to vent (unscaled).

mation on the island are missing. Filling this gap is the principal aim of the following section.

### 3.2. Data, Methods, and Model Adjustments

[26] Using the methodology described above, we fit ground deformation data obtained at 10 stations using data from continuously recording dual frequency GPS receivers.

The stations were distributed at a radial distance between 1.6 and 9.6 km from the vent (Figure 5). Data were collected at a frequency of 0.033 Hz using Dorn-Margolin Choke Ring antennas. Post-processing was performed using the GIPSY software employing final, precise satellite orbits, clocks, and Earth orientation parameters (see *Jansma and Mattioli* [2005] for details). Site velocities were tied to an external

frame (Caribbean Plate [*DeMets et al.*, 2007]). 3-D position estimates at each site were obtained by averaging dual-frequency, code and phase observations for a single 24 h period. This data set covers a period of continuous inflation in its entirety, lasting from mid-July 2003 to November 2005, as well as the subsequent deflationary period, which lasted from December 2005 to March 2007. Site velocities were calculated assuming linear behavior over the period of interest and component velocity errors include contributions from white, colored and random walk noise sources. For both eruption periods, recorded displacements and measure uncertainties from the individual stations are given in Figure 5.

[27] For the first time period, it is notable that records from the station closest to the source center (HERM) deviate markedly from the overall displacement pattern. However, it already has been recognized earlier that data recorded at HERM do not generally agree with observations from neighboring GPS sites (Montserrat Volcano Observatory (MVO), personal communication, 2006). As the location of HERM is in the immediate vicinity of the volcanic center, the GPS records can be explained with local effects due to dome loading on English Crater wall [*Norton et al.*, 2002]. We hence exclude data from this site from further analyses. In addition, the first data set includes two single data points, which also differ from the overall deformation pattern (TRNT at  $U_z$  and SOUF at  $U_r$ ). Data from the deflationary episode show that the amplitude of horizontal displacements  $U_r$  gradually increases with increasing distance from SHV. The only exception here is found for records from TRNT. The spatial distribution of the vertical displacements reveals unexpectedly large subsidence at stations at the east flank of the volcano (HARR, HERM, TRNT, WTYD), while stations from all other parts of the island show overall deformation pattern as in the previous deformation period, with a gradual decrease of vertical displacements with distance to the vent. We hence will split the second data set and exclude the records from stations located at the east flank of SHV from our modeling. All other data will be used for the modeling of source parameters of the deep reservoir. We will not give a detailed analyses of the different deformation changes at the eastern flank of SHV as compared to the overall deformation pattern of the island, as all interpretations would be purely speculative based on the low number of available data. Preliminary results on the possible influence of faulting are summarized in Text S1 in the auxiliary material.<sup>1</sup> In oncoming studies, however, we will additionally evaluate data from more recent deformation periods and will then analyze the entire deformation field in a full 3-D domain in order to find possible scenarios that explain the anomaly of the SHV eastern flank in the deformation records.

[28] Accounting for an average network elevation of 250 m (ellipsoidal height) and crustal heterogeneities from this datum downward, we performed a series of forward models, in which we varied the source depth between 8 and 14 km in steps of 0.5 km, in order to find the best fit solution to the recorded data. Source geometries explored for the simulation included spherical, oblate and prolate shapes for all investigated depths. For quantification of the model fit, all

results were evaluated using the method of root mean square error (RMSE).

### 3.3. Results

[29] We first analyzed the direction and length of the horizontal displacement vectors in the recorded cGPS data, in order to determine the horizontal position of the pressure source with respect to GPS benchmarks. The data indicated that in both of the investigated time periods, the displacement originated from a source that was located about 640 m  $\pm$  150 m to the NE of the vent. Whether or not to include data from sites yielding lower observational precision in the analysis does not significantly affect the results with respect to the inferred horizontal source location. Plotting the observed displacement versus radial distance from source shows a very clear pattern for either investigated time period (Figure 6).

[30] Figure 6 illustrates results from the best fit models for each period using both horizontal and vertical displacements. For inflation (2003–2005), our results show an excellent fit for a source centered between 11.5 and 12 km below sea level, with a moderately prolate ( $0.7 < a/c < 0.8$ ) geometry. For deflation (2005–2007), we found the best fitting model to contain a source located at a depth of about 13  $\pm$  0.5 km below sea level with a slightly more prolate geometry ( $a/c = 0.6$ ). The RMSE is similar for model results within the given ranges for source depth and eccentricity, but markedly increases for models with source parameters outside these ranges. For the deflationary time period the RMSE is slightly lower than for the inflation (RMSE = 0.107 for ground inflation, while RMSE = 0.0904 for ground deflation). This difference, however, is due to the large derivation of TRNT at  $U_z$  and SOUF at  $U_r$  during ground inflation, but it gives no constraints on the choice of the preferred source model. Additionally accounting for topography and second-order heterogeneities (i.e., lateral heterogeneities; including a zone of denser material located between 1.5 and 3 km below sea level (bsl) and the shallow magma chamber (accounting for compliant material) centered at 6 km bsl) has only a very minor impact on the results (Figure S2 in the auxiliary material), as these applications yield only a slight decrease in source eccentricity  $a/c$  by 0.1.

[31] As the magnitude of the observed surface displacement depends non-uniquely on both the pressure changes in the magma body and its size, we run additional FE models to test a range of source volumes in order to determine corresponding pressure changes. We applied source volumes between 4 and 52 km<sup>3</sup>, consistent with estimates of the SHV magma chamber volume from analysis of deformation data [*Voight et al.*, 2006; *Elsworth et al.*, 2008]. Thus far nearly 1 km<sup>3</sup> of andesite lava has erupted and models of magma chamber discharge during extrusive eruptions [*Blake*, 1981; *Huppert and Woods*, 2002] show that the chamber volume is substantially larger than the extruded volume. This suggests a chamber volume of several km<sup>3</sup> at least and may be a few tens of km<sup>3</sup>. For sources between 4 and 52 km<sup>3</sup> we found resulting pressure changes  $\Delta P$  in the range of 625  $\pm$  40 MPa to 50  $\pm$  3 MPa (with larger overpressure values for smaller source volumes and vice versa) for the 2003–2005 inflation. These values compare to pressure changes of 745  $\pm$  55 MPa to 60  $\pm$  5 MPa for the deflationary episode between 2005 and 2007.

<sup>1</sup>Auxiliary materials are available in the HTML. doi:10.1029/2009JB006909.

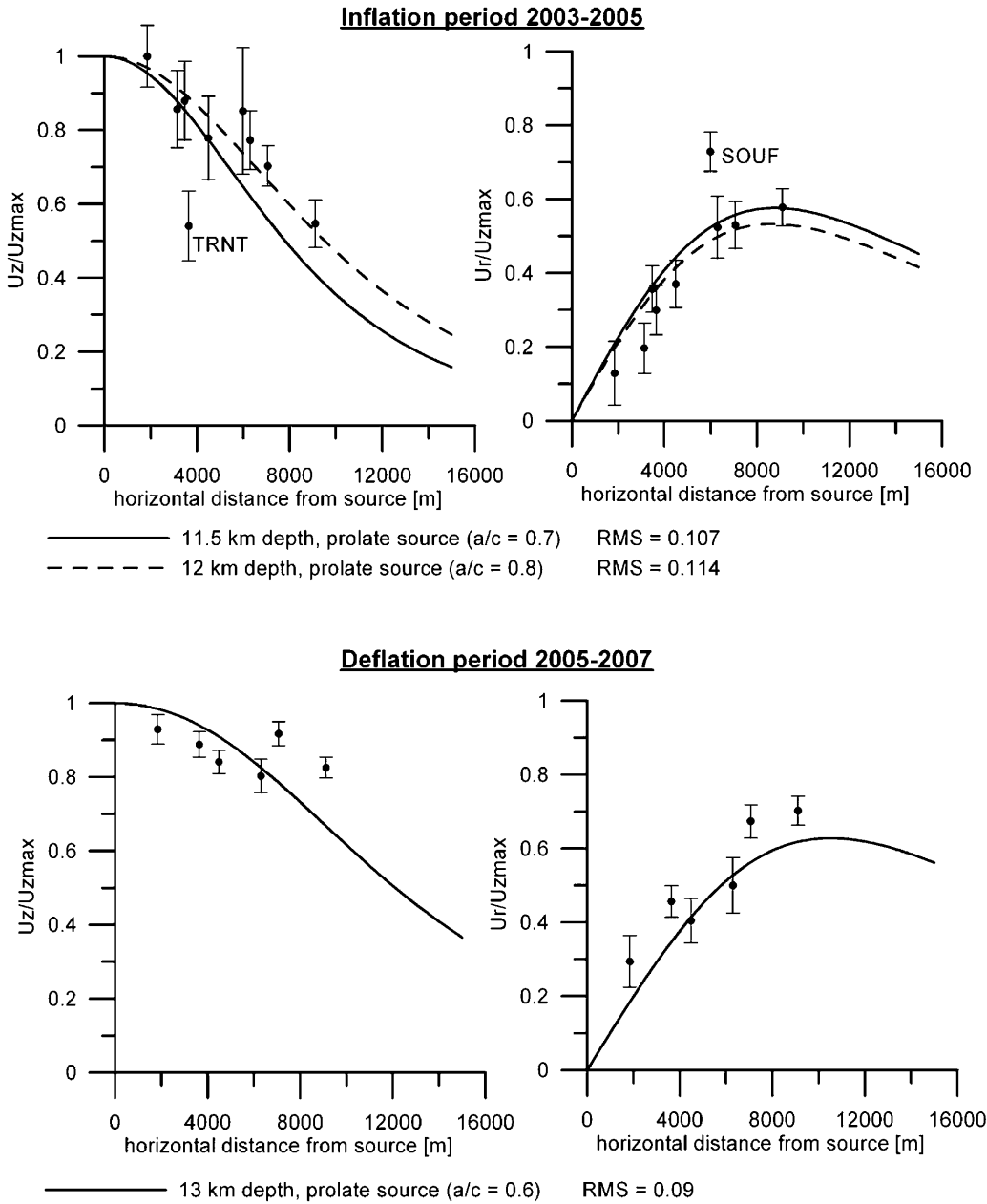


**Figure 6.** Best fit of the recorded data to results predicted by our heterogeneous deformation model. The inferred source depth is found to be (top) 11.5–12 km below sea level for deformation data recorded between 2003 and 2005 and (bottom) 13 km below sea level for data recorded between 2005 and 2007. For both activity periods, the source geometry giving the best fit of model to data is a prolate spheroid ( $a/c = 0.6$  to  $0.8$ ). Error bars represent 1 sigma data uncertainties.

### 3.4. Discussion of Source Characteristics

#### 3.4.1. Inferred Source Depth and Geometry

[32] We found that the model with the lowest RMSE is for a prolate ( $0.6 < a/c < 0.8$ ) magma reservoir located about 640 m NE of the active SHV vent. The source is centered in the middle crust between 11.5 and 13 km below sea level.

[33] Our results on source location and depth are in good agreement with results derived from inverting for a spherical source embedded in an HOHS [Mattioli and Herd, 2003; Mattioli, 2005; Elsworth et al., 2008]. This agreement is

rather unexpected, as our theoretical work (Figure 4) predicts an underestimation of source depth when using the simplified homogeneous model. Considering a wide range of spheroidal geometries the best fitting source has a slightly prolate geometry compared to the spherical shape proposed by Elsworth et al. [2008]. Based on the analysis of cGPS data, Voight et al. [2008] suggested that the deep magma reservoir is a prolate spheroid with  $a/c = 0.5$  that is centered at 10 km depth. Considering the mismatch derived from their simplified assumption of a homogeneous medium (underestimation in depth and a prolate source geometry

with higher eccentricity), their results are in a good agreement with the source characteristics we inferred when accounting for mechanical heterogeneities.

### 3.4.2. Source Dimension Versus Pressure Change

[34] Estimates of pressure changes in magma chambers during eruption on Montserrat and other andesitic dome volcanoes are between 1 and 20 MPa [Stasiuk *et al.*, 1993; Voight *et al.*, 2006]. Our models, however, show that a source volume  $V$  between 4 and 52 km<sup>3</sup> requires an order of magnitude higher pressure variations to match observed data than is consistent with the tensile strength of crustal rocks, which is widely considered as limit of magma chamber overpressures. This misfit would also apply for the work of Elsworth *et al.* [2008], who state a volume of  $V = 4$  km<sup>3</sup> for the deep magma reservoir embedded in a homogeneous elastic medium. They assume a shear modulus  $\mu$  of 1 GPa (based on strain-measured surface loading from the 13 July 2003 ash accumulation and cGPS-measured surface uplift from dome surcharge removal [see Voight *et al.*, 2006]), which translates to a pressure change of 30 MPa. However, we now believe that their chosen value for the shear modulus is underestimated given the available seismic data as shown in Figure 1. Employing a more realistic value with  $\mu = 30$  GPa (average shear modulus of the upper crust (10 km) as deduced from the velocity profile) would equally yield overpressure values at an order of magnitude higher than reasonable to fit the deformation records.

[35] Note that there is a discussion in literature on the discrepancies between elastic rock properties derived from seismic, ground deformation and laboratory studies, although King [1969] noted that the discrepancies are particularly significant for shallow regions of the crust. On the basis of deformation data analysis, Hooper *et al.* [2002] constrained the shear modulus of the upper crust of Kilauea Volcano (upper 2.7 km) to be a factor of 5 lower than inferred from a  $P$ -wave velocity profile [Okubo *et al.*, 1997]. Beauducel *et al.* [2000] modeled the lava dome static weight to determine the rigidity values of the summit rocks at Merapi Volcano as considerably lower than obtained from seismic velocities. The authors explained the low rigidity values in the volcanic edifice with high fracturing of mostly uncompacted rocks near the surface. However, while low rigidity values near the surface certainly need to be accounted for in ground deformation studies on shallow pressure sources, the influence of a surface layer with less stiffly responding rocks is becoming significantly lower when modeling ground deformation triggered by a deep seated magma chamber (compare with results of Geyer and Gottsmann [2010]). Hence, for the case of SHV, where the pressure source is centered at midcrustal depths, the influence of a possible less stiffly responding surface layer that has not been adequately resolved in the seismic velocity profile, should be only very minor and not capable of explaining the mismatch between physically realistic and model-derived values of pressure changes in the deep reservoir. Hence, in order to investigate this mismatch, we now explore alternative mechanical scenarios.

#### 3.4.2.1. Mechanically Compliant Source Region

[36] It appears a viable assumption that a magmatic ("hot") zone exists at depths greater than 10 km, which is in contrast to our assumption of increasing stiffness with depth to a value of  $E = 105$  GPa at  $z > 10$  km, would result in a

soft zone with lower values for the Young's Modulus. In order to explore this scenario, we incorporated a mechanically soft and compliant layer with  $E = 10$  GPa at  $10 < z < 15$  km in our model. Results show that for source volumes between 4 and 52 km<sup>3</sup>, resulting pressure variations are between 205 and 25 MPa (inflationary episode) and 245 and 46 MPa (deflationary episode), respectively (Table 1). Although, these values appear more realistic in particular for the larger source dimensions, they are still in the upper range of what is plausible for SHV. While a mechanically compliant lithology at greater depths beneath SHV seems geologically plausible and could help explain the observed deformation data, we find that such a zone does not fully eliminate the observed misfit between source pressure change and volume.

#### 3.4.2.2. Volumetric Changes of the Source and the Influence of Magma Compressibility

[37] Geodetic data from actively erupting volcanoes enable comparison of inferred source volume changes with erupted volumes of volcanic material. The dense rock equivalent (DRE) of magma extruded at SHV during the investigated deflationary episode (December 2005 to February 2007) was  $2.1 \times 10^8$  m<sup>3</sup> (MVO, personal communication, 2007). According to Tiampo *et al.* [2000], the volume change  $\Delta V_{deform}$  of a prolate spheroid that is surrounded by a homogeneous medium at depths greater than twice the semi-major axis,  $c$ , can be related via

$$\Delta V_{deform} = \frac{\Delta P c a^2 \pi}{\mu} \quad (2)$$

where  $\mu$  is the shear modulus at depth. This model does not consider the compressibility of the magma and is the volume change associated with deformation of the chamber walls. We evaluate volume changes for high and low shear moduli  $\mu$  at source depth. Note we vary  $\mu$  at the source depth only, and maintain the heterogeneity of the overlying material as shown in Figure 1. Thus,  $\Delta P^* V$  and  $\mu$  are not related as they would be in a purely homogeneous medium, as the ratio  $\Delta P^* V / \mu$  is not constant. We apply the product of pressure change and chamber volume obtained for the time period December 2005 to March 2007 using our FE method (see Table 1). For a medium with a typical shear modulus of crustal rocks at  $\mu = 40$  GPa, the estimated volume change for the deflationary period is  $6.1 \pm 0.2 \times 10^7$  m<sup>3</sup>, which is much lower by a factor of 3.4 than the observed DRE lava output. However, if we choose  $\mu = 4$  GPa at source depth a volume change of  $3.4 \pm 1.4 \times 10^8$  m<sup>3</sup> is calculated, which is more consistent with the observations. Here we note that Elsworth *et al.* [2008] also used a very low shear modulus (1 GPa) in their models. One possible explanation for having to invoke a very low shear modulus for the host rocks at midcrustal depths is that a large soft zone of hot crust surrounds the magma chamber. However, there are no laboratory measurements of shear modulus of crustal rocks even at high temperature that support such low values. We therefore explore the alternative idea that magma compressibility allows eruption of larger volumes (as also demonstrated by Johnson *et al.* [2000] and Rivalta and Segall [2008] for the case of Kilauea Volcano and Afar) and that neglecting magma compressibility gives an underestimate of the shear modulus needed to make the ground deformation and observed lava volume consistent with one another via

**Table 1.** Applied Parameters and Inferred Source Properties

Parameter	Description	Value
$\beta$	magma compressibility ( $\text{Pa}^{-1}$ )	$0.25\text{--}3 \times 10^{-10}$
$\eta$	viscosity ( $\text{Pa s}$ )	$10^{17}$
$\mu$	shear modulus ( $\text{Pa}$ )	$15 \times 10^9$ for viscoelastic medium; for elastic medium, see $E$
$\nu$	Poisson's ratio	0.25
$E$	Young's modulus ( $\text{Pa}$ )	$17 \times 10^9 \leq E \leq 102 \times 10^9$ at $-0.5 \leq z \leq 10$ case 1: $E = 105 \times 10^9$ (equals $\mu = 40 \times 10^9$ ) at $z > 10$ case 2: $E = 10 \times 10^9$ (equals $\mu = 4 \times 10^9$ ) at $z > 10$ $320 \times 10^6$ at $z = 12$
$P_l$	lithostatic pressure ( $\text{Pa}$ )	
$\Delta P$	pressure change in source ( $\text{MPa}$ )	
$V$	source volume ( $\text{km}^3$ )	
$V_e$	DRE erupted during 2005–2007 deflation ( $\text{m}^3$ )	$2.1 \times 10^8$
$\Delta V_{\text{compress}}$	volume magma efflux as to magma compressibility ( $\text{m}^3$ )	$0.3\text{--}4.0 \times 10^7$
$\Delta V_{\text{deform}}$	volume magma efflux as to dike wall deformation ( $\text{m}^3$ )	$6.1 \pm 0.2 \times 10^7$ for $E = 105 \times 10^9$ at $z > 10$ $3.4 \pm 1.4 \times 10^8$ for $E = 10 \times 10^9$ at $z > 10$
$z$	depth (km), positive downward with $z = 0$ at sea level	
Inferred overpressure values and source dimensions		
2003–2005 ground inflation		
For $E = 105 \times 10^9$ at $z > 10$		$624 \geq \Delta P \geq 50$ for $4 \leq V \leq 52$
For $E = 10 \times 10^9$ at $z > 10$		$205 \geq \Delta P \geq 25$ for $4 \leq V \leq 52$
Accounting for viscoelasticity		
2005–2007 ground deflation		
For $E = 105 \times 10^9$ at $z > 10$		$85 \geq \Delta P \geq 14$ for $8 \leq V \leq 50$
For $E = 10 \times 10^9$ at $z > 10$		$745 \geq \Delta P \geq 60$ for $4 \leq V \leq 52$
Accounting for magma compressibility		
		$245 \geq \Delta P \geq 46$ for $4 \leq V \leq 52$
		$\Delta P = 20$ for $8 \leq V \leq 153$

equation (2). Magma compressibility allows additional magma volume to be erupted as first recognized by *Blake* [1981]. The compressibility of silicate melts is higher than crystalline phases typically by factors of several [Bottinga, 1985; *Webb*, 1997] and further, as explored by *Huppert and Woods* [2002], the compressibility can increase markedly with the presence of exsolved volatiles in volatile saturated magma. The surface efflux related to compressibility of the magma  $\Delta V_{\text{compress}}$  can be calculated via

$$\Delta V_{\text{compress}} = \beta P_l V_e \quad (3)$$

where the magma compressibility  $\beta$  is the reciprocal of the bulk modulus  $K$ ,  $P_l$  is the lithostatic pressure at depth and  $V_e$  is the amount of magma extruded from the reservoir. Note that this model accounts for magma flux due to magma compressibility only, but not for volume changes during deformation. Values of the bulk modulus for silicate melts are typically in the range 5 to 20 GPa [*Webb*, 1997]. Assessing the role of exsolved volatiles is more difficult as the volatile content and composition of the SHV magma is less constrained. Water contents of 4.5% to 5% are found in melt inclusions [*Devine et al.*, 1998] and provide a minimum value. The magma can still be saturated at 11 km if there are modest amounts of poorly soluble  $\text{SO}_2$  and  $\text{CO}_2$  present [*Carroll and Holloway*, 1994]. We illustrate the potential for very compressible volatile-saturated bubbly magma by considering a total water content of 6.5 wt % and 2000 ppm  $\text{CO}_2$ , which is oversaturated at 320 MPa with about 1.8 wt %  $\text{H}_2\text{O}$  exsolved. These chosen values are consistent with data on fumarole chemistry at SHV [*Hamrouya et al.*, 1998] and melt inclusion data. Using the

equations of *Huppert and Woods* [2002], the bulk modulus of the multiphase magma (accounting for melt, volatiles, bubbles and crystals) would be about 2.65 GPa at 11 km depth. This value is several factors lower than that of the silicate melt, which itself is more compressible than the crust. Our calculations and derived results are in good agreement with a study applied to Mount St. Helens [*Mastin et al.*, 2008]. Only difference is that the calculations presented by *Mastin et al.* [2008] are based on the assumption of a lower water content in the magma, which might be reasonable for Mount St. Helens, but is probably not appropriate for arc andesites as appearing at SHV. The compressibility of the magma system could be increased further if the main deep magma chamber were well-connected to the shallower chamber, where the density derivative for the magma with pressure is larger. Note here that, for the same bulk water content, the exsolved water content at 120 MPa (~5 km magma chamber) is only slightly different due to the buffering effects of  $\text{CO}_2$ , but the bulk modulus reduces to 0.4 GPa. The deep chamber will thus become significantly more compressible by being connected to the shallow chamber, even though the primary cause of surface deformation is sourced in the deep system.

[38] Taking a range of magma compressibilities of  $0.25\text{--}3 \times 10^{-10} \text{ Pa}^{-1}$  and a lithostatic pressure  $P_l = 320 \text{ MPa}$ , the deduced volume of surface efflux related to magma compressibility is  $0.3\text{--}4.0 \times 10^7 \text{ m}^3$ . This range of magma efflux is slightly below the calculated values of elastic source volume change calculated from the deformation using a bulk modulus of 40 GPa, and is most consistent with a more compressible magma system. What this shows then is that the observations can be reconciled with a crust with a normal

shear modulus and an important role for magma compressibility. The model is most consistent if there is exsolved gas throughout a well-connected magmatic system.

[39] Hence, the total volume of erupted magma can be calculated by adding the (1) elastic volume decrease of the magma chamber as associated with depressurization ( $6.1 \pm 0.2 \times 10^7 \text{ m}^3$ ) and (2) the volume of surface efflux as a result of magma decompression ( $0.3\text{--}4.0 \times 10^7 \text{ m}^3$ ). The finite chamber size can be re-calculated by accounting for magma compressibility using equation (3), converted to

$$V = \frac{\Delta V_{\text{deform}} + \Delta V_{\text{compress}}}{\Delta P \beta} \quad (4)$$

For magma compressibilities between 0.25 and  $3 \times 10^{-10} \text{ Pa}^{-1}$ , total magma flux volumes between 6.2 and  $10.3 \times 10^7 \text{ m}^3$ , and a depressurization of 20 MPa, the resulting chamber size is in a range between 8 and  $153 \text{ km}^3$ ; sources of up to  $50 \text{ km}^3$  seem to be realistic for SHV.

### 3.4.2.3. Viscoelasticity of Host Rock

[40] Another viable deep source mechanism is the time-dependent behavior of surrounding host rock. Viscoelastic behavior of a medium can induce ground deformation with source pressure changes significantly lower than the case for an elastic medium, while maintaining the same footprint of ground deformation [e.g., Bonafede *et al.*, 1986; De Natale and Pingue, 1996; Folch *et al.*, 2000].

[41] We perform a first order approximation of the possible influence of viscoelasticity on rock deformation at SHV to test its influence on derived pressure transients using the approach presented by Dragoni and Manganensi [1989]. Their analytical model solves for ground deformation as a function of time induced by pressure changes in a spherical magma chamber, surrounded by a concentric, spherical, viscoelastic shell in an elastic medium. This model approach has also been applied in the analysis of deformation data from Long Valley Caldera [Newman *et al.*, 2001]. Considering a viscoelastic medium, Folch *et al.* [2000] demonstrated numerically that the larger the eccentricity of a spheroidal source, the larger its influence on the deformation amplitude. Significant differences in resultant patterns compared to spherical sources are found for eccentricities of  $a/c \leq 0.5$  [see also Newman *et al.*, 2006]. Given that the pressurization of a spheroidal source with low eccentricity compared to a spherical source in a viscoelastic medium affects only slightly the magnitude of predicted deformation, but not the overall deformation pattern, we solve for time-dependent deformation assuming a spherical source shape. Clearly, the assumption of mechanical homogeneity in the Dragoni and Manganensi [1989] solution is limiting, nonetheless results should offer a first order approximation of the possible influence of viscoelastic behavior on the observed ground deformation.

[42] The displacement  $u_r$  as a function of distance from the source  $r$  and time  $t$  is defined by

$$u_r(r, t) = \frac{1}{4} \frac{\Delta P r_s^3}{\mu r^2} \left[ 1 - \left( 1 - \frac{r_c^3}{r_s^3} \right) \right] e^{-t/\tau} \quad (5)$$

where  $r_c$  is the distance from the source center to the source wall,  $r_s$  is the distance between source center and the wall of the viscoelastic shell and  $\mu$  is the shear modulus of the

viscoelastic shell. The Maxwell relaxation time for a system is

$$\tau = \frac{9}{5} \frac{\eta}{\mu} \left( \frac{r_s}{r_c} \right)^3 \quad (6)$$

where  $\eta$  is the viscosity of the surrounding shell. Assuming  $\eta = 10^{17} \text{ Pa s}$  and  $\mu = 15 \text{ GPa}$ , we accounted for thicknesses of the viscoelastic shell  $r_s$  between 20% and 100% of source radius  $r_c$ . We further assumed a source radius and overpressure values at the upper range of what is realistic with  $R_I = 2000$  and  $\Delta P = 20 \text{ MPa}$  to simulate the 2.3 years of uplift with a net maximum amplitude of 7.8 cm at SHV. For a small sized shell ( $r_s/r_c = 0.2$ ) we found that uplift reaches its maximum of 3.2 cm after 2.3 years (while  $U_{z\text{max}} = 1.8 \text{ cm}$  for the initial elastic response at  $t = 0$ ; Figure 7). For  $r_s/r_c = 0.7$ , 7.8 cm of uplift is predicted after 2.3 years, and a maximum of 9.5 cm is reached after 6 years.  $r_s/r_c = 1$  yields a ground uplift of 9 cm after 2.3 years. Remarkable uplift is predicted for another 7 years reaching a maximum of approximately 14.7 cm.

[43] The recorded time series data from SHV [cf. Elsworth *et al.*, 2008, Figure 2] does not allow us to deduce a time-dependent response due to the substantial noise in the data. It is important, however, to note that the period of ground inflation between 2003 and 2005 was directly followed by an episode of ground deflation, which again appears to be triggered from the same pressure source. Though ongoing time-dependent uplift could have been superseded by subsidence, it follows that the greater the influence of time-dependence on the recorded uplift (that is, the longer the relaxation time of the system) the higher the required depressurization of the system to induce overall ground deflation as observed in the 2005–2007 records. Hence, the influence of viscoelasticity needs to be both large enough to fit the magnitude of recorded ground deformation and simultaneously small enough to roughly correlate with the 2 to 3 years cyclicity of ground inflation/deflation. Our results show that these conditions are met for  $r_s/r_c = 0.7$  and  $\eta = 10^{17} \text{ Pa s}$ . For viscosities an order of magnitude higher or lower resulting strains would either not be observable or stresses would be relaxed over the investigation period, respectively. For source volumes between 8 and  $50 \text{ km}^3$  (as seem to be realistic values for SHV that are also in agreement with source volume estimates derived from calculations of magma compressibility), the required overpressure to fit the recorded ground inflation data is between 85 and 14 MPa.

[44] Our preferred volume-overpressure pair for conditions explored above is a reservoir source volume of  $32 \text{ km}^3$  with an overpressure of 20 MPa to explain ground deformation recorded during the 2003–2005 ground inflation at SHV. This first order approximation shows that accounting for both magma compressibility and time-dependent rheology of the source region yields acceptable and realistic source characteristics.

### 3.4.3. Coupling of Shallow and Deep Magma Reservoir

[45] Observations from other volcanic areas such as Yellowstone [Wicks *et al.*, 1998] and Hekla [Linde *et al.*, 1993] revealed that magmatic stressing can be triggered simultaneously by multiple reservoirs in a magmatic system. This entails that either the entire magmatic system can be equally

**time-dependent uplift due to visco-elastic rheology**

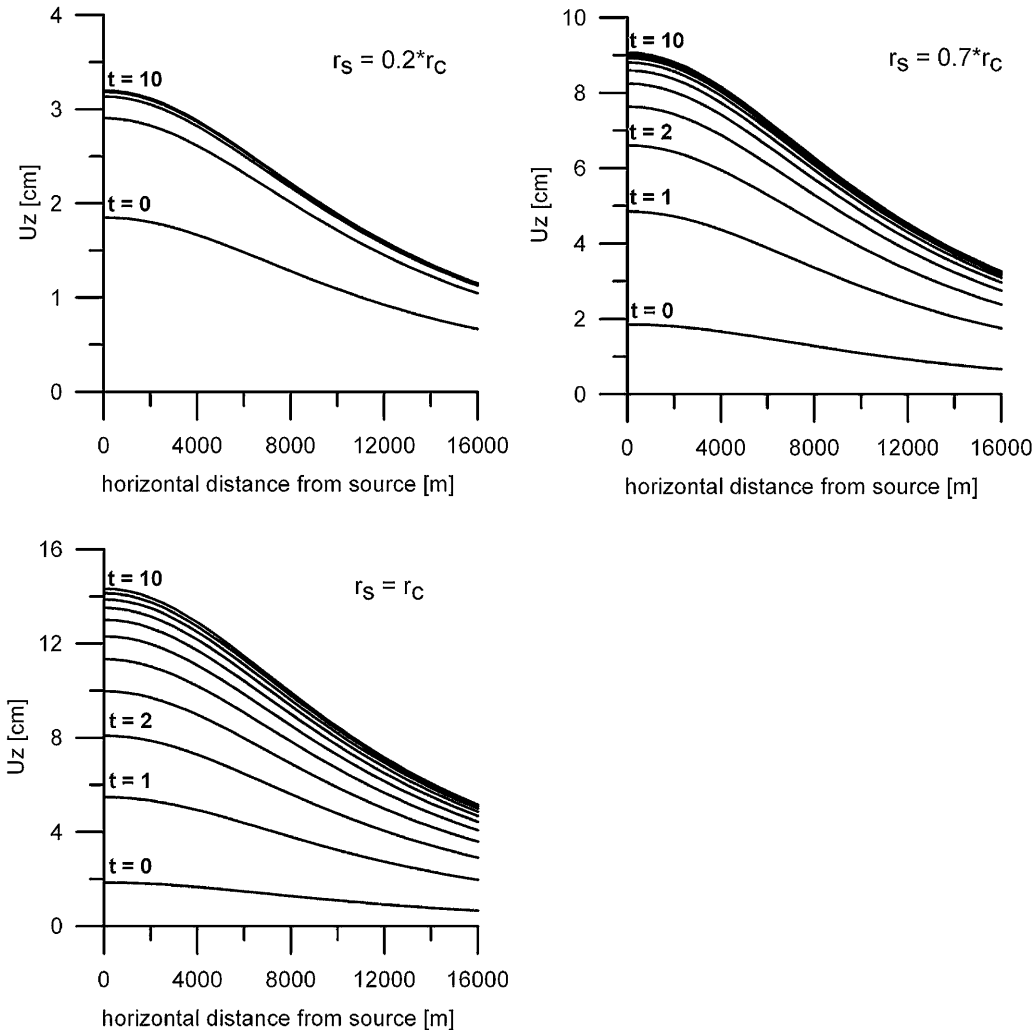


**Figure 7.** Quantification of time-dependent uplift induced by a viscoelastic shell that is surrounding a spherical magma chamber with  $r_c = 2$  km and  $P = 25$  MPa. Results show deformation within 10 years for a shell with  $\eta = 10^{17}$  Pa s and varying thickness of the shell  $r_s$  of 20%, 70%, and 100% of the magma chamber radius. A contribution of viscoelastic rheology as given by a shell with 0.7 times the radius of the magma chamber best explains the ground deformation observed at SHV.

pressurized/depressurized or that the shallow and the deep magma bodies can have a reverse pressurization, due to a degassing of the lower chamber and an accumulation of gases in the upper chamber. As the behavior of the magmatic system at SHV is consistent with a shallow and a deep magma reservoir [Murphy et al., 2000; Elsworth et al., 2008], we investigated the deformation pattern that is generated when the entire system is closed in order to quantify a possible influence of the upper magma chamber during the herein analyzed deformation periods. We constrained the shallow magma chamber to be of spherical shape centered at 6 km depth as suggested in earlier works [e.g., Mattioli et al., 1998; Voight et al., 2006]. For the deep reservoir we considered a range of different geometries and depths. We further investigated the effect of different volume ratios of the two sources.

[46] Our results show that in the case of equal pressurization/depressurization of the entire system the volume ratio of both chambers controls the length of the lateral distance between source centers and maximum horizontal ground deformation, while the amplitude of horizontal ground deformation is controlled by the depth and geometry of the deep source (Figure 8a). We found that when accounting for two magma chambers the radius of the deep magma chamber needs to be at minimum 4 times larger than the radius of the upper chamber in order to roughly fit with the overall deformation pattern that has been recorded on Montserrat. In particular, for the inflationary time period the two source model gives best fit with the recorded data when considering the same parameters for the deep magma chamber as inferred from the single source model (11.5–12 km depth, prolate geometry with  $0.7 < a/c < 0.8$ ). How-

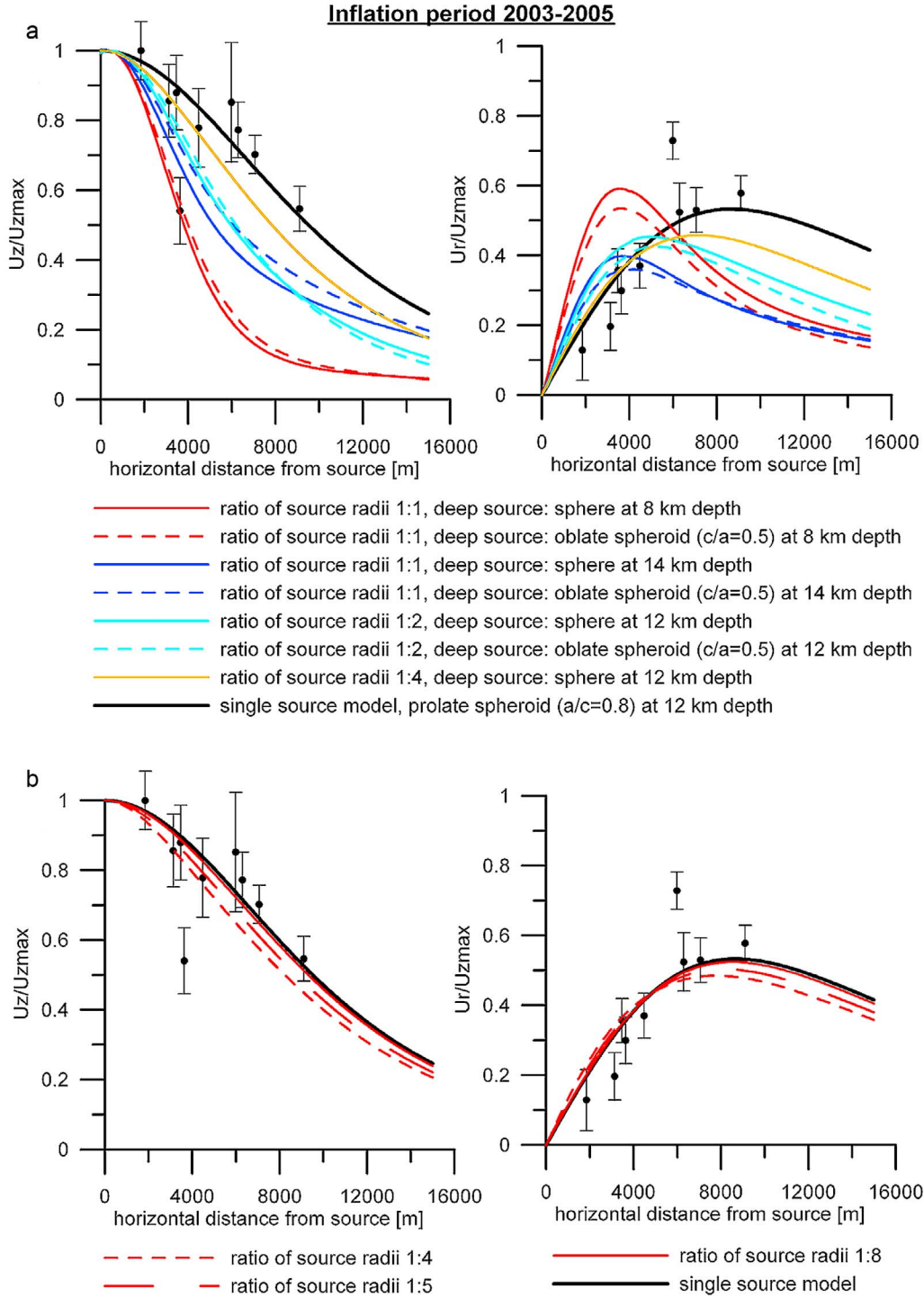


**Figure 8.** Normalized results of surface deformation due to equal pressurization of a magmatic system with two sources. (a) Shallow source is assumed to be of spherical shape centered at 6 km below sea level. Source parameters of the deep reservoir are varied as followed: solid line, spherical geometry; dashed line, oblate geometry ( $c/a = 0.5$ ); red, source depth 8 km, ratio of source radii 1:1; dark blue, source depth 14 km, ratio of source radii 1:1; light blue, source depth 12 km, ratio of source radii 1:2; yellow, source depth 12 km, ratio of source radii 1:4. (b) Prolate source geometry ( $a/c = 0.8$ ), source depth 12 km. The ratio of source radii is 1:4 (dotted line), 1:5 (dashed line), and 1:8 (solid red line). Data from the 2003–2005 ground inflation and the best fit as inferred from a single source model (prolate source ( $a/c = 0.8$ ) at 12 km depth) are given for comparison (in black).

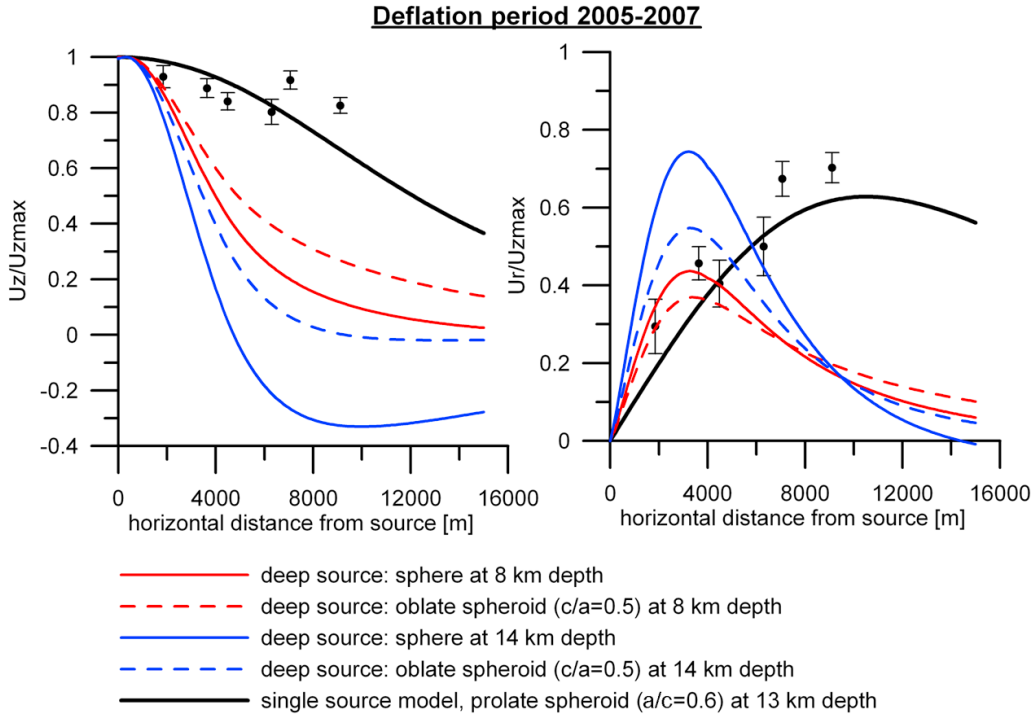


**Figure 9.** Normalized results of surface deformation due to reverse pressurization of two sources. The shallow source is assumed to be of spherical shape centered at 6 km below sea level. Volume ratio of the sources is 1:1. Source parameters of the deep reservoir are varied as followed: solid line, spherical geometry; dashed line, oblate geometry ( $c/a = 0.5$ ); red, source depth 8 km; dark blue, source depth 14 km. Data from the 2005–2007 ground deflation and the best fit as inferred from a single source model (prolate source ( $a/c = 0.6$ ) at 13 km depth) are given for comparison (in black).

ever, in order to yield a satisfactory fit quality the radii of the sources (shallow and deep chamber) need to have a minimum ratio of 1:8 (Figure 8b). This value, however, seems unrealistic as it would imply that even for a shallow magma chamber with a volume of  $0.5 \text{ km}^3$ , the deep reservoir has a minimum dimension of  $270 \text{ km}^3$ .

[47] When considering a reverse pressurization (upper source  $+\Delta P$ , lower source  $-\Delta P$ ) of the two chambers, the pressure strength ( $\Delta P * V$ ) needs to be equal for both sources in order to account for a net mass preservation. It follows that, in contrast to the scenario described above (overall pressurization of the entire system), changes in the source volume ratio involve that pressure changes vary accordingly different at each of the sources and hence, do not affect the overall deformation pattern. Comparing the predicted deformation for reverse pressurization of the two magma chambers with the recorded 2005–2007 ground deflation data, we found a large misfit in the results on both the horizontal and the vertical component (Figure 9). Thus, we exclude reverse pressurization of two magma chambers as causative scenario for the 2005–2007 ground deflation.

[48] Based on our results we suggest that the 2003–2005 ground inflation and the 2005–2007 ground deflation were triggered by the deep magma chamber only. In the time of inflation the lower system was likely to be closed by a blockage either at the bottom of the upper chamber or in the conduit that connects the two reservoirs. The subsequent onset of ground deflation was a consequence of pressure release in the deeper chamber, triggered by an opening of

the blockage. Note that this model requires the shallow magma chamber and the upper dike-conduit to be open. It should be pointed out, however, that this scenario does not necessarily explain the other periods of ground deformation that were observed at SHV, as the conditions probably were different in earlier times of the eruption, when the shallow magma chamber was more active.

#### 4. Summary and Conclusions

[49] We investigated the effect of mechanical heterogeneity as opposed to homogeneity of crustal rocks on ground deformation due to pressurization of midcrustal sources of different geometries. Our initial generic study is applicable to explain surface deformation on volcanic arc-islands and offers an approach to explore associated source characteristics. Our results showed that (1) the horizontal displacement is markedly amplified by mechanical heterogeneity for spherical sources, (2) the maximum horizontal deformation at the free surface occurs closer to the source in a heterogeneous medium, (3) the footprint of vertical surface deformation is shorter in a heterogeneous medium, and (4) disparities in model solutions for either mechanical framework are in general greater for prolate sources compared to oblate source geometries.

[50] We applied our model on recorded ground deformation data from Soufrière Hills Volcano, Montserrat, in order to constrain source characteristics of the deep magma reservoir and hence, to image the complex structure of the

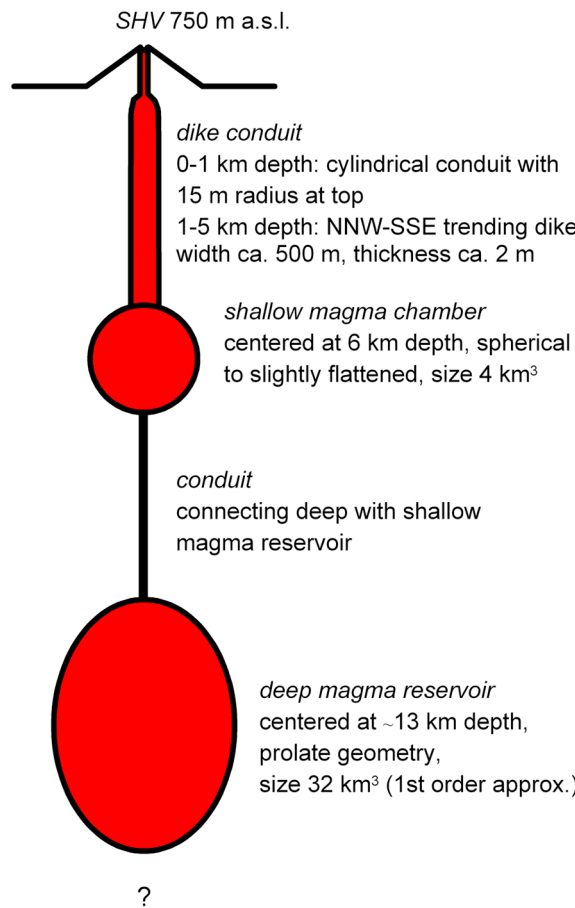


**Figure 10.** Sketch of the proposed structure of the magmatic system beneath Soufrière Hills Volcano.

SHV magmatic system (Figure 10). Our best fitting midcrustal magma chamber has a slightly prolate spheroidal geometry centered approximately 640 m NE of the vent at 11.5–13 km below sea level. Calculations on source dimensions and related overpressure values indicate that so far unexplored thermomechanical conditions in the midcrust may have a major influence on the scale of surface deformation. Our results hint toward a low rigidity layer in the intermediate crust and/or toward viscoelastic behavior of rocks in proximity to the main zone of melt accumulation.

[51] Accounting for magma compressibility, a magma body with a minimum volume of 8 km<sup>3</sup> being depressurized by 20 MPa provides the most consistent model to explain the reported volume of extruded dense rock material. Our favorite model to explain the documented ground inflation involves a source volume of 32 km<sup>3</sup>, pressurized by 20 MPa and surrounded by a viscoelastic shell with a radius of 1400 m. Our first-order exploration of the parameter domain (source dimensions and internal pressure changes) to explain the recorded deformation data does not claim to be exhaustive, but to provide a quantitative basis to simultaneously incorporate crustal heterogeneity, magma compressibility and time-dependent rheology in future modeling.

[52] **Acknowledgments.** S.H. acknowledges funding by the Bavarian Research Foundation (BFS DPA-53/05). J.G. was supported by grants from

the Natural Environmental Research Council (NE/E007961/1) and the Royal Society (UF051396). This work is a result of partial support from the National Science Foundation under awards NSF-CD-0607691, NSF-CD-0507334, and NSF-CD-0607782. The CALIPSO Facility was supported by NSF-IF-0523097 and NSF-IF-0732728. This support is gratefully acknowledged. The conclusions reported here are those of the authors. We thank the staff of the Montserrat Volcano Observatory (MVO) for operation and maintenance of the cGPS network over the years and provision of erupted lava volume data. We are grateful to M. Paulatto for providing the velocity model. The comments of two anonymous reviewers were helpful to improve the paper and are greatly acknowledged.

## References

- Anderson, M. E. (1936), Dynamics and formation of cone-sheets, ring-dykes, and cauldron-subsidence, *Trans. R. Soc. Edinburgh*, 56, 128–157.
- Annen, C., J. D. Blundy, and R. S. J. Sparks (2006), The genesis of intermediate and silicic magmas in deep crustal hot zone, *J. Petrol.*, 47(3), 505–539, doi:10.1093/petrology/egi084.
- Barclay, J., M. Rutherford, M. R. Carroll, M. D. Murphy, J. D. Devine, J. Gardner, and R. S. J. Sparks (1998), Experimental phase equilibria constraints on preeruptive storage conditions of the Soufrière Hills magma, *Geophys. Res. Lett.*, 25(18), 3437–3440, doi:10.1029/98GL00856.
- Battaglia, M., and P. Segall (2004), The interpretation of gravity changes and crustal deformation in active volcanic areas, *Pure Appl. Geophys.*, 161, 1453–1467, doi:10.1007/s00024-004-2514-5.
- Beauducel, F., F. H. Cornet, E. Suhanto, T. Duquesnoy, and M. Kasser (2000), Constraints on magma flux from displacements data at Merapi volcano, Java, *J. Geophys. Res.*, 105(B4), 8193–8203, doi:10.1029/1999JB900368.
- Bianchi, R., A. Coradini, C. Federico, G. Giberti, G. Sartori, and R. Scandone (1984), Modelling of surface ground deformations in the Phlegraean Fields volcanic area, Italy, *Bull. Volcanol.*, 47(2), 321–330, doi:10.1007/BF01961563.
- Bianchi, R., A. Coradini, C. Federico, G. Giberti, P. Lanciano, J. P. Pozzi, G. Sartori, and R. Scandone (1987), Modeling of surface deformation in volcanic areas: The 1970–1972 and 1982–1984 crises of Campi Flegrei, Italy, *J. Geophys. Res.*, 92(B13), 14,139–14,150, doi:10.1029/JB092iB13p14139.
- Blake, S. (1981), Volcanism and the dynamics of open magma chambers, *Nature*, 289, 783–785, doi:10.1038/289783a0.
- Bonacorso, A., S. Cianetti, C. Giunchi, E. Trasatti, M. Bonafede, and E. Boschi (2005), Analytical and 3-D numerical modeling of Mt. Etna (Italy) volcano inflation, *Geophys. J. Int.*, 163, 852–862, doi:10.1111/j.1365-246X.2005.02777.x.
- Bonafede, M., M. Dragoni, and F. Quarenì (1986), Displacement and stress fields produced by a center of dilation and by a pressure source in a viscoelastic half-space: Application to the study of ground deformation and seismic activity at Campi Flegrei, Italy, *Geophys. J. R. Astron. Soc.*, 87, 455–485.
- Bottinga, Y. (1985), On the isothermal compressibility of silicate melts at high pressure, *Earth Planet. Sci. Lett.*, 74, 350–360, doi:10.1016/S0012-821X(85)80007-8.
- Carroll, M. R., and J. R. Holloway (Eds.) (1994), *Volatiles in Magma*, Rev. Mineral., vol. 30, Mineral. Soc. of Am., Washington, D. C.
- Cayol, V., and F. H. Cornet (1998), Effects of topography on the interpretation of the deformation field of prominent volcanoes—Application to Etna, *Geophys. Res. Lett.*, 25(11), 1979–1982, doi:10.1029/98GL1512.
- Cervelli, P. F., and M. L. Coombs (2006), Variations in deformation rate and magma composition at Augustine Volcano, Alaska: A mechanical account of the 2006 eruptions, *Eos Trans. AGU*, 87(52), Fall Meet. Suppl., Abstract V42B-07.
- Codina, R., and A. Folch (2004), A stabilized finite element predictor-corrector scheme for the incompressible Navier-Stokes equations using a nodal based implementation, *Int. J. Numer. Methods Fluids*, 44, 483–503, doi:10.1002/fld.648.
- Costa, A., O. Melnik, and R. S. J. Sparks (2007a), Control of conduit geometry and wallrock elasticity on lava dome eruptions, *Earth Planet. Sci. Lett.*, 260, 137–151, doi:10.1016/j.epsl.2007.05.024.
- Costa, A., O. Melnik, R. S. J. Sparks, and B. Voight (2007b), Control of magma flow in dykes on cyclic lava dome extrusion, *Geophys. Res. Lett.*, 34, L02303, doi:10.1029/2006GL027466.
- Couch, S., R. S. J. Sparks, and M. R. Carroll (2003), The kinetics of degassing-induced crystallization at Soufrière Hills Volcano, Montserrat, *J. Petrol.*, 44(8), 1477–1502, doi:10.1093/petrology/44.8.1477.
- De Barros, L., H. A. Pederson, J. P. Métaxian, C. Valdés-Gonzalez, and P. Lesage (2008), Crustal structure below Popocatépetl Volcano (Mexico) from analysis of Rayleigh waves, *J. Volcanol. Geotherm. Res.*, 170, 5–11, doi:10.1016/j.jvolgeores.2007.09.001.

- DeMets, C., G. S. Mattioli, P. Jansma, R. Rogers, C. Tenorios, and H. L. Turner (2007), Present motion and deformation of the Caribbean plate: Constraints from new GPS geodetic measurements from Honduras and Nicaragua, in *Geologic and Tectonic Development of the Caribbean Plate in Northern Central America*, edited by P. Mann, *Spec. Pap. Geol. Soc. Am.*, 428, 21–36, doi:10.1130/2007.2428(02).
- De Natale, G., and F. Pingue (1993), Ground deformations in collapsed caldera structures, *J. Volcanol. Geotherm. Res.*, 57, 19–38, doi:10.1016/0377-0273(93)90029-Q.
- De Natale, G., and F. Pingue (1996), Ground deformation modeling in volcanic areas, in *Monitoring and Mitigation of Volcano Hazards*, edited by R. Scarpa and R. I. Tilling, pp. 365–388, Springer, Berlin.
- Devine, J. D., M. D. Murphy, M. J. Rutherford, J. Barclay, R. S. J. Sparks, M. R. Carroll, S. R. Young, and J. E. Gardner (1998), Petrologic evidence for pre-eruptive pressure-temperature conditions, and recent reheating of andesitic magma erupting at the Soufrière Hills Volcano, Montserrat, W.I., *Geophys. Res. Lett.*, 25(19), 3669–3672, doi:10.1029/98GL01330.
- Devine, J. D., M. J. Rutherford, G. E. Norton, and S. R. Young (2003), Magma storage region processes inferred from geochemistry of Fe-Ti oxides in andesitic magma, Soufrière Hills Volcano, Montserrat, W.I., *J. Petrol.*, 44(8), 1375–1400, doi:10.1093/petrology/44.8.1375.
- Dieterich, J. H., and R. W. Decker (1975), Finite element modeling of surface deformation associated with volcanism, *J. Geophys. Res.*, 80(29), 4094–4102, doi:10.1029/JB080i029p04094.
- Dragoni, M., and C. Manganensi (1989), Displacement and stress produced by a pressurized, spherical magma chamber, surrounded by a viscoelastic shell, *Phys. Earth Planet. Inter.*, 56, 316–328, doi:10.1016/0031-9201(89)90166-0.
- Elsworth, D., G. Mattioli, J. Taron, B. Voight, and R. Herd (2008), Implications of magma transfer between multiple reservoirs on eruption cycling, *Science*, 322, 246–248, doi:10.1126/science.1161297.
- Fernández, J., and J. B. Rundle (1994), FORTRAN program to compute displacement, potential and gravity changes resulting from a magma intrusion into a multilayered Earth model, *Comput. Geosci.*, 20(4), 461–510, doi:10.1016/0098-3004(94)90079-5.
- Fernández, J., K. F. Tiampo, and J. B. Rundle (2001), Viscoelastic displacement and gravity changes due to point magmatic intrusions in a gravitational layered solid earth, *Geophys. J. Int.*, 146, 155–170, doi:10.1046/j.0956-540x.2001.01450.x.
- Fialko, Y., Y. Khazan, and M. Simons (2001), Deformation due to a pressurized horizontal circular crack in an elastic half-space, with application to volcano geodesy, *Geophys. J. Int.*, 146, 181–190, doi:10.1046/j.1365-246X.2001.00452.x.
- Folch, A., and J. Gottsmann (2006), Faults and ground uplift at active calderas, in *Mechanisms of Activity and Unrest at Large Calderas*, edited by C. Troise, G. De Natale, and C. R. J. Kilburn, *Geol. Soc. Spec. Publ.*, 269, 109–120.
- Folch, A., J. Fernández, J. B. Rundle, and J. Martí (2000), Ground deformation in a viscoelastic medium composed of a layer overlying a half space: A comparison between point and extended sources, *Geophys. J. Int.*, 140, 37–50, doi:10.1046/j.1365-246x.2000.00003.x.
- Geyer, A., and J. Gottsmann (2010), The influence of mechanical stiffness on caldera deformation and implications for the 1971–1984 Rabaul uplift (Papua New Guinea), *Tectonophysics*, 483, 399–412, doi:10.1016/j.tecto.2009.10.029.
- Hammouya, G., P. Allard, P. Jean-Baptiste, F. Parello, M. P. Semet, and S. R. Young (1998), Pre- and syn-eruptive geochemistry of volcanic gases from Soufrière Hills of Montserrat, West Indies, *Geophys. Res. Lett.*, 25(19), 3685–3688, doi:10.1029/98GL02321.
- Hautmann, S., J. Gottsmann, R. S. J. Sparks, A. Costa, O. Melnik, and B. Voight (2009), Modelling ground deformation caused by oscillating overpressure in a dyke conduit at Soufrière Hills Volcano, Montserrat, *Tectonophysics*, 471, 87–95, doi:10.1016/j.tecto.2008.10.021.
- Hooper, A., P. Segall, K. Johnson, and J. Rubinstein (2002), Reconciling seismic and geodetic models of the 1989 Kilauea south flank earthquake, *Geophys. Res. Lett.*, 29(22), 2062, doi:10.1029/2002GL016156.
- Huppert, H. E., and A. W. Woods (2002), The role of volatiles in magma chamber dynamics, *Nature*, 420, 493–495, doi:10.1038/nature01211.
- Jansma, P. E., and G. S. Mattioli (2005), GPS results from Puerto Rico and the Virgin Islands: Constraints on the tectonic setting and rates of active faulting, in *Active Tectonics and Seismic Hazards of Puerto Rico, the Virgin Islands, and Offshore Areas*, edited by P. Mann, *Spec. Pap. Geol. Soc. Am.*, 385, 13–30.
- Johnson, D. J., F. Sigmundsson, and P. T. Delaney (2000), Comment on “Volume of magma accumulation or withdrawal estimated from surface uplift or subsidence, with application to the 1960 collapse of Kilauea volcano” by P. T. Delaney and D. F. McTigue, *Bull. Volcanol.*, 61, 491–493, doi:10.1007/s004450050006.
- King, M. S. (1969), Static and dynamic elastic moduli of rocks under pressure, *Proc. U.S. Symp. Rock Mech.*, 11th, 329–351.
- Linde, A. T., K. Ágústsson, I. S. Sacks, and R. Stefánsson (1993), Mechanism of the 1991 eruption of Hekla from continuous borehole strain monitoring, *Nature*, 365, 737–740, doi:10.1038/365737a0.
- Linde, A. T., S. Sacks, D. Hidayat, and B. Voight (2008), The Montserrat Soufrière Hills explosion of March 2004: Magma geometry and incompressibility from borehole strain data, *Eos Trans. AGU*, 89(53), Fall Meet. Suppl., Abstract V53C-02.
- Manconi, A., T. R. Walter, and F. Amelung (2007), Effects of mechanical layering on volcano deformation, *Geophys. J. Int.*, 170, 952–958, doi:10.1111/j.1365-246X.2007.03449.x.
- Masterlark, T. (2007), Magma intrusion and deformation predictions: Sensitivity to the Mogi assumptions, *J. Geophys. Res.*, 112, B06419, doi:10.1029/2006JB004860.
- Mastin, L. G., E. Roeloffs, N. M. Beeler, and J. E. Quick (2008), Constraints on the size, overpressure, and volatile content of the Mount St. Helens Magma system from geodetic and dome growth measurements during the 2004–2006+ Eruption, in *A Volcano Rekindled: The Renewed Eruption of Mount St. Helens*, edited by D. R. Sherrod, W. E. Scott, and P. H. Stauffer, *U.S. Geol. Surv. Prof. Pap.*, 1750, 461–488.
- Mattioli, G. S. (2005), CALIPSO and a decade of GPS surface deformation: What we have learned from Soufrière Hills Volcano, Montserrat, paper presented at Soufrière Hills Volcano—Ten Years On Scientific Conference, Seismic Res. Unit, Univ. of West Indies, Montserrat.
- Mattioli, G. S., and R. Herd (2003), Correlation of GPS geodesy with surface magma flux at Soufrière Hills Volcano, Montserrat, *Séismol. Res. Lett.*, 74(2), 230.
- Mattioli, G., T. H. Dixon, F. F. Farina, E. S. Howell, P. E. Jansma, and A. L. Smith (1998), GPS measurement of surface deformation around Soufrière Hills Volcano, Montserrat, from October 1995 to July 1996, *Geophys. Res. Lett.*, 25(18), 3417–3420, doi:10.1029/98GL00931.
- McTigue, D. F. (1987), Elastic stress and deformation near a finite spherical magma body: Resolution of the point source paradox, *J. Geophys. Res.*, 92(B12), 12,931–12,940, doi:10.1029/JB092iB12p12931.
- Mogi, K. (1958), Relations between the eruptions of various volcanoes and the deformations of the ground surfaces around them, *Bull. Earthquake Res. Inst. Univ. Tokyo*, 36, 99–134.
- Murphy, M. D., R. S. J. Sparks, J. Barclay, M. R. Carroll, and T. S. Brewer (2000), Remobilization of andesite magma by intrusion of mafic magma at the Soufrière Hills Volcano, Montserrat, West Indies, *J. Petrol.*, 41(1), 21–42, doi:10.1093/petrology/41.1.21.
- Newman, A. V., T. H. Dixon, G. I. Ofoegbu, and J. E. Dixon (2001), Geodetic and seismic constraints on recent activity at Long Valley Caldera, California: Evidence for viscoelastic rheology, *J. Volcanol. Geotherm. Res.*, 105, 183–206, doi:10.1016/S0377-0273(00)00255-9.
- Newman, A. V., T. H. Dixon, and N. Gourmelen (2006), A four-dimensional viscoelastic deformation model for Long Valley Caldera, California, between 1995 and 2000, *J. Volcanol. Geotherm. Res.*, 150, 244–269, doi:10.1016/j.jvolgeores.2005.07.017.
- Norton, G. E., et al. (2002), Pyroclastic flow and explosive activity at Soufrière Hills Volcano, Montserrat, during a period of virtually no magma extrusion (March 1998 to November 1999), in *The Eruption of Soufrière Hills Volcano, Montserrat, From 1995 to 1999*, edited by T. H. Druitt and B. P. Kokelaar, *Geol. Soc. Mem.*, 21, 467–481.
- Okada, Y. (1985), Surface deformation due to shear and tensile faults in a halfspace, *Bull. Seismol. Soc. Am.*, 75, 1135–1154.
- Okubo, P. G., H. M. Benz, and B. A. Chouet (1997), Imaging the crustal magma sources beneath Mauna Loa and Kilauea volcanoes, Hawaii, *Geology*, 25, 867–870, doi:10.1130/0091-7613(1997)025<0867:ITCMSB>2.3.CO;2.
- Paulatto, M., et al. (2010), Upper crustal structure of an active volcano from refraction/reflection tomography, Montserrat, Lesser Antilles, *Geophys. J. Int.*, 180, 685–696, doi:10.1111/j.1365-246X.2009.04445.x.
- Poland, M., M. Hamburger, and A. Newman (2006), The changing shapes of active volcanoes: History, evolution, and future challenges for volcano geodesy, *J. Volcanol. Geotherm. Res.*, 150, 1–13, doi:10.1016/j.jvolgeores.2005.11.005.
- Pritchard, M. E., and M. Simons (2004), An InSAR-based survey of volcanic deformation in the central Andes, *Geochem. Geophys. Geosyst.*, 5, Q02002, doi:10.1029/2003GC000610.
- Rivalta, E., and P. Segall (2008), Magma compressibility and the missing source for some dike intrusions, *Geophys. Res. Lett.*, 35, L04306, doi:10.1029/2007GL032521.
- Rundle, J. B. (1980), Static elastic-gravitational deformation of a layered half space by point couple sources, *J. Geophys. Res.*, 85, 5355–5363, doi:10.1029/JB085iB10p05355.
- Rutherford, M. J., and J. D. Devine (2003), Magmatic conditions and magma ascent as indicated by hornblende phase equilibria and reactions

- in the 1995–2002 Soufrière Hills magma, *J. Petrol.*, **44**(8), 1433–1453, doi:10.1093/petrology/44.8.1433.
- Saito, G., K. Uto, K. Kazahaya, H. Shinohara, Y. Kawanabe, and H. Satoh (2005), Petrological characteristic and volatile content of magma from the 2000 eruption of Miyakejima Volcano, Japan, *Bull. Volcanol.*, **67**, 268–280, doi:10.1007/s00445-004-0409-z.
- Sparks, R. S. J., M. Murphy, A.-M. Lejeune, R. Watts, J. Barclay, and S. Young (2000), Control on the emplacement of the andesite lava dome of the Soufrière Hills Volcano, Montserrat by degassing-induced crystallization, *Terra Nova*, **12**, 14–20, doi:10.1046/j.1365-3121.2000.00267.x.
- Stasiuk, M. V., C. Jaupart, and R. S. J. Sparks (1993), On the variations of flow-rate in non-explosive lava eruptions, *Earth Planet. Sci. Lett.*, **114**, 505–516, doi:10.1016/0012-821X(93)90079-O.
- Sudo, Y., and L. S. L. Kong (2001), Three dimensional seismic velocity structure beneath Aso Volcano, Kyushu, Japan, *Bull. Volcanol.*, **63**, 326–344, doi:10.1007/s004450100145.
- Tiampo, K. F., J. B. Rundle, J. Fernández, and J. O. Langbein (2000), Spherical and ellipsoidal volcanic sources at Long Valley caldera, California, using a genetic algorithm inversion technique, *J. Volcanol. Geotherm. Res.*, **102**, 189–206, doi:10.1016/S0377-0273(00)00185-2.
- Trasatti, E., C. Giunchi, and M. Bonafede (2003), Effects of topography and rheological layering on ground deformation in volcanic regions, *J. Volcanol. Geotherm. Res.*, **122**, 89–110, doi:10.1016/S0377-0273(02)00473-0.
- Trasatti, E., C. Giunchi, and M. Bonafede (2005), Structural and rheological constraints on source depth and overpressure estimates at the Campi Flegrei Caldera, Italy, *J. Volcanol. Geotherm. Res.*, **144**, 105–118, doi:10.1016/j.jvolgeores.2004.11.019.
- Trasatti, E., C. Giunchi, and N. Piana Agostinetti (2008), Numerical inversion of deformation caused by pressure sources: Application to Mount Etna (Italy), *Geophys. J. Int.*, **172**, 873–884, doi:10.1111/j.1365-246X.2007.03677.x.
- Voight, B., et al. (2006), Unprecedented pressure increase in deep magma reservoirs triggered by lava-dome collapse, *Geophys. Res. Lett.*, **33**, L03312, doi:10.1029/2005GL024870.
- Voight, B., et al. (2008), Conundrum on magmatic reservoir of Soufrière Hills volcano, Montserrat: Enigmatic evidence and the case for a vertically elongated reservoir, *Eos Trans. AGU*, **89**(53), Fall Meet. Suppl., Abstract V53C-08.
- Wadge, G., G. S. Mattioli, and R. A. Herd (2006), Ground deformation at Soufrière Hills Volcano, Montserrat during 1998–2000 measured by radar interferometry and GPS, *J. Volcanol. Geotherm. Res.*, **152**, 157–173, doi:10.1016/j.jvolgeores.2005.11.007.
- Webb, S. L. (1997), Silicate melts: Relaxation, rheology and the glass transition, *Rev. Geophys.*, **35**, 191–218, doi:10.1029/96RG03263.
- Wicks, C., Jr., W. Thatcher, and D. Dzurisin (1998), Migration of fluids beneath Yellowstone Caldera inferred from satellite radar interferometry, *Science*, **282**, 458–462, doi:10.1126/science.282.5388.458.
- Williams, C. A., and G. Wadge (1998), The effects of topography on magma deformation models: Application to Mt. Etna and radar interferometry, *Geophys. Res. Lett.*, **25**, 1549–1552, doi:10.1029/98GL01136.
- Yang, X. M., P. Davis, and J. H. Dietrich (1988), Deformation from inflation of a dipping finite prolate spheroid in an elastic half-space as a model for volcanic stressing, *J. Geophys. Res.*, **93**(B5), 4249–4257, doi:10.1029/JB093iB05p04249.

---

J. Gottsmann, S. Hautmann, and R. S. J. Sparks, Department of Earth Sciences, University of Bristol, Wills Memorial Building, Queen's Road, Bristol, BS8 1RJ, UK. (j.gottsmann@bristol.ac.uk; stefanie.hautmann@googlemail.com; steve.sparks@bristol.ac.uk)

G. S. Mattioli, Department of Geosciences, University of Arkansas, 113 Ozark Hall, Fayetteville, AR 72701, USA. (mattioli@uark.edu)

I. S. Sacks, Department of Terrestrial Magnetism, Carnegie Institution of Washington, 52541 Broad Branch Rd., NW, Washington, DC 20015-1305, USA. (sacks@dtm.ciw.edu)

M. H. Strutt, British Geological Survey, Kingsley Dunham Centre, Keyworth NG12 5GG, UK. (mhst@bgs.ac.uk)